

# 1 Addition of brackish water to tundra soils does not inhibit 2 methane production: implications for Arctic coastal methane 3 production

4 **Alexie Roy-Lafontaine**<sup>1, 5</sup>, Rebecca Lee<sup>2</sup>, Peter M.J. Douglas<sup>3, 4</sup>, Dustin Whalen<sup>2</sup>, André  
5 Pellerin<sup>1,5</sup>

6 <sup>1</sup>Institut des Sciences de la Mer de Rimouski, Université du Québec à Rimouski, Rimouski, Québec, Canada et Centre  
7 de recherche Geotop

8 <sup>2</sup>Geological Survey of Canada, Natural Resources Canada, Halifax, Nova Scotia, Canada

9 <sup>3</sup>Department of Earth and Planetary Sciences and Geotop Research Centre, McGill University, Montréal, Québec,  
10 Canada

11 <sup>4</sup>Centre d'Études Nordiques, Université Laval, Québec, Québec, Canada

12 <sup>5</sup>Québec Océan, Université Laval, Québec, Québec, Canada

13 *Correspondence to:* Alexie Roy-Lafontaine (alexieroylafontaine@gmail.com)

14 **Abstract.** In Arctic regions where coastal sediments contain permafrost, global climate change drives processes such  
15 as erosion and subsidence. The contribution of these processes to carbon emissions, especially from ground  
16 subsidence, are still uncertain. Relative sea level rise can lead to more waterlogged environments, promoting anoxic  
17 degradation of organic matter but it can also lead to a greater exposure of coastal sediments to seawater. This could  
18 alter methane (CH<sub>4</sub>) production dynamics, although the controls remain poorly understood. For instance, sulfates  
19 contained in seawater may have a tampering effect on methanogenesis through competitive inhibition but the increase  
20 in microbial abundance could enhance methanogenesis. In this study, we present CH<sub>4</sub> production rates alongside  
21 geochemical analyses in a rapidly evolving coastal landscape near the community of Tuktoyaktuk, NWT, Canada,  
22 which is located in the continuous permafrost zone. To better constrain CH<sub>4</sub> production dynamics along the land to  
23 ocean continuum, sediment cores were collected from nearshore marine sediments and soil profiles were collected  
24 from the active layer of the coastal (intertidal) zone and inland soils. Anoxic incubations were performed, amended  
25 with brackish water to simulate the effect of seawater on the breakdown of organic matter and the production of CH<sub>4</sub>.  
26 We found marine sediments expectedly led to negligible CH<sub>4</sub> production rates, while the inland sites showed variable  
27 rates between null and 35 nmol cm<sup>-3</sup> d<sup>-1</sup>. The coastal (intertidal) zone had the highest rates reaching 415 nmol cm<sup>-3</sup> d<sup>-1</sup>.  
28 Interestingly, sulfate present in brackish water and sediments did not suppress methanogenesis in the incubations of  
29 the coastal and inland zones. Analyses of stable carbon isotopes from CH<sub>4</sub> produced in the incubation experiment  
30 indicated greater acetotrophy and higher organic matter lability in the coastal zone, possibly contributing to higher  
31 CH<sub>4</sub> production rates. This study highlights the potential for significant CH<sub>4</sub> emissions even with high sulfate  
32 concentrations which are classically thought to inhibit methanogenesis. This suggests that Arctic coastal microbial  
33 CH<sub>4</sub> production might be an understudied source to the atmosphere.

## 34 **1 Introduction**

35 Arctic coastal ecosystems are impacted by sea level rise, coastal erosion, land submersion, higher frequency in storm  
36 events and permafrost degradation (AMAP 2019; Guimond et al., 2021; Irrgang et al., 2022; Lantuit et al., 2013; Lim  
37 et al., 2020). The amplification of coastal environmental changes has impacts on biogeochemical cycles (AMAP,  
38 2017) and on organic matter (OM) degradation processes and fluxes at the land-ocean continuum (Tanski et al., 2021).  
39 Furthermore, the progressive thawing of permafrost exposes long frozen organic matter to microbial decomposition  
40 (Lapham et al., 2020; Pellerin et al., 2022; Schuur et al., 2015), leading to the release of greenhouse gases like carbon  
41 dioxide (CO<sub>2</sub>) and methane (CH<sub>4</sub>). Inputs and outputs of the Arctic carbon biogeochemical cycle are known to be  
42 reshaped by rapid environmental changes (Couture et al., 2018), but processes in coastal settings are still poorly  
43 understood.

44 Rates of coastal change vary according to the morphology of coastal landscapes (Manson et al., 2019). The  
45 average rate of land retreat measured in the Tuktoyaktuk Coastlands (North-West Territories, Canada), our study site,  
46 between 1985 and 2020 was -1.06 m/yr, while processes of ground subsidence and submersion induced retreat rates  
47 higher than -4 m/yr (Costa, 2022) which can inundate large swaths of land. Inundated tundra flats and polygons are  
48 widespread landforms in the landscape (Costa, 2022). Polygon tundra flats are characterized by ice-wedge polygons,  
49 which are formed by the repeated thermal contraction and expansion of the upper layers of the permafrost (Steedman  
50 et al., 2016). At the surface, the polygons are expressed as minor topographic features separated by lower-lying, often  
51 wet or inundated channels called troughs (Fig 1). Polygons can be classified as low-centered (with a low, wet center  
52 and raised rims) or as high-centered (with well-drained centers and lower well-drained rims) (Fig 1), exhibiting strong  
53 thermal, hydrological and geochemical gradients (Vaughn et al., 2016).

54 During growing season, where atmospheric temperatures allow for active layer to thaw and vegetation to  
55 grow, hydrological conditions in polygons play a pivotal role in shaping the pathways of OM decomposition and  
56 consequently influence the resulting CO<sub>2</sub> and CH<sub>4</sub> production. Well drained oxic conditions allow microbes to  
57 decompose OM rapidly, leading to the production of CO<sub>2</sub> (Jones et al., 2020). Conversely, water saturation restricts  
58 oxygen availability, promoting anaerobic respiration and fermentation, inducing both CO<sub>2</sub> and CH<sub>4</sub> production  
59 (Lipson et al., 2012; Turetsky et al., 2008). Thus, coastal changes and higher atmospheric temperatures during open-  
60 water season can swiftly alter water saturation conditions in polygons, in many cases significantly enhancing  
61 fermentation and CH<sub>4</sub> production (Elberling et al., 2013; Holm et al., 2020; Treat et al., 2015).

62 Furthermore, coastal changes can also influence the chemistry of the water within soils, which can affect OM  
63 degradation. In anaerobic conditions, OM degradation processes follow a sequence of electron acceptors of decreasing  
64 energetic yields with nitrate, manganese oxides, iron oxides and sulfate as the most abundant electron acceptors  
65 (Froelich et al., 1979). It is when all alternative electron acceptors are depleted that fermentation takes place, leading  
66 to the production of CH<sub>4</sub>; methanogenesis. For example, it has long been established that in beach, estuarine, and  
67 marsh mudflats on the Brittany coast (France), organic matter (OM) degradation is dominated by sulfate reduction, as  
68 the high sulfate content of seawater inhibits methanogenesis through competitive inhibition (Winfrey and Ward,

69 1983). In contrast, sediments beneath thermokarst lakes are anoxic and largely devoid of alternative electron acceptors,  
70 so OM degradation is almost entirely driven by methanogenesis (Sepulveda-Jauregui et al., 2015). These examples  
71 highlight that the chemical composition of the aqueous environment plays a critical role in controlling the pathways  
72 of OM degradation. CH<sub>4</sub> produced in soils or sediments can also be oxidized by anaerobic methanotrophic archaea  
73 and sulfate-reducing bacteria (Boetius et al., 2000; La et al., 2022) present in the soils or sediment, contributing to  
74 lower CH<sub>4</sub> emissions in coastal environments. Thus, on or near the coast, the interaction with seawater, which contains  
75 electron acceptors such as sulfate, can shift the OM mineralization pathway and the resulting CO<sub>2</sub> and CH<sub>4</sub>  
76 productions. Consequently, a nuanced understanding of biogeochemical processes and their drivers is paramount in  
77 determining the magnitude of permafrost carbon emissions, especially from coastal environments.

78 Numerous CH<sub>4</sub> emissions monitoring programs are in operation, but remote-sensing methods lack the ability  
79 to comprehensively capture the microbial, biogeochemical and environmental processes involved. In specific regions,  
80 estimates of methane production from the breakdown of OM is possible by carefully studying degradation pathways  
81 and production rates (Pellerin et al., 2022; Heslop et al., 2015; Knoblauch et al., 2018; Treat et al., 2014). To reduce  
82 the knowledge gap of CH<sub>4</sub> biogeochemistry in coastal permafrost settings, we collected material from the active layer  
83 and taliks of water bodies for incubation experiments, which were coupled to physical and chemical characterizations.  
84 The main objective of this study was to assess microbial CH<sub>4</sub> production dynamics in a coastal permafrost setting and  
85 apply it at the landscape level, since methane production is well documented in inland thermokarst but is not well  
86 understood in a land-ocean interaction context. We hypothesized that methanogenesis in coastal active layer  
87 incubations would be suppressed by the addition of sulfate. Consequently, we discuss the influence of environmental  
88 conditions on microbial CH<sub>4</sub> production with an emphasis on brackish water addition in coastal soils and sediments  
89 along with the microbial pathways involved. We then apply these results at the landscape level to provide an estimate  
90 of CH<sub>4</sub> production in the event that a natural process like a storm inputs brackish water over a large area of polygonal  
91 patterned ground. We use the region around Tuktoyaktuk as an example.

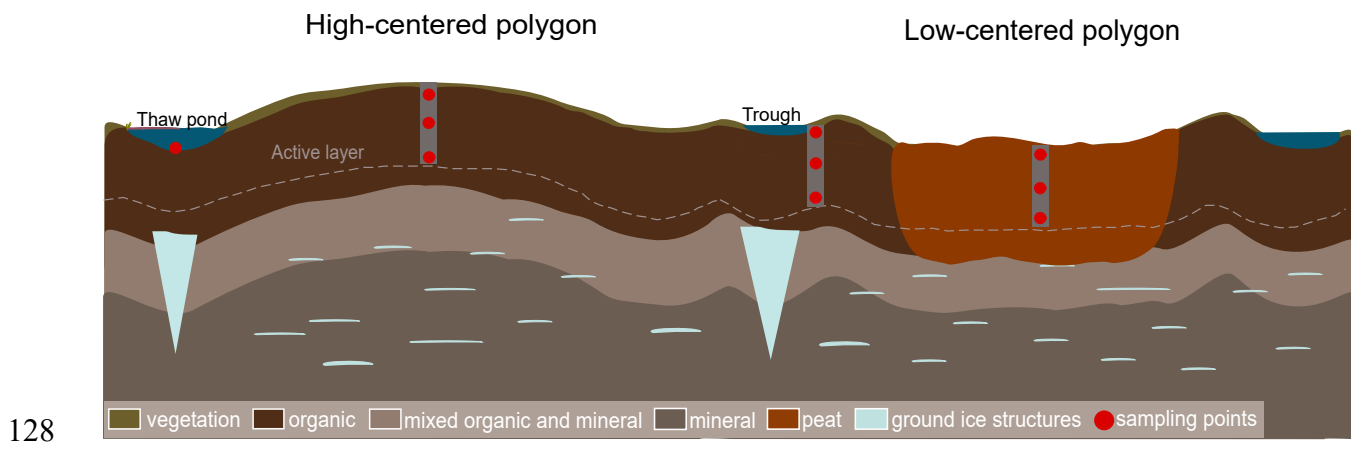
## 92 **2 Methods**

### 93 **2.1 Site description and sampling**

94 Tuktoyaktuk (69°26'24'' N, 133°01'52''W) is located in the Inuvik region of the North-West Territories,  
95 adjacent to the Arctic Ocean in the Kugmallit Bay, east of the Mackenzie Delta. The region experiences prolonged  
96 cold winters, short cool summers, and year-round low precipitation, fostering low-arctic tundra vegetation. Lying in  
97 the continuous permafrost zone, its coastal areas feature thick Quaternary and glaciogenic unconsolidated deposits  
98 (Rampton, 1988), where permafrost thickness averages 400 m (Hu et al., 2013) and is characterized by prevalent  
99 ground ice structures (Mackay and Dallimore, 1992; Martin et al., 2018; Murton, 1996; Rampton, 1988). The area  
100 has been ice-free for the past 13 000 years, with evidence indicating that early Holocene summer temperatures were  
101 up to 6°C warmer than today, fostering vegetation and peat accumulation (Dallimore et al., 1997; Vardy et al., 1997).  
102 During that same period, sea level was considerably lower than it is today and the Tuktoyaktuk area was located  
103 approximately 100 km inland (Vardy et al., 1997). Currently, ground subsidence and coastal erosion are major causes

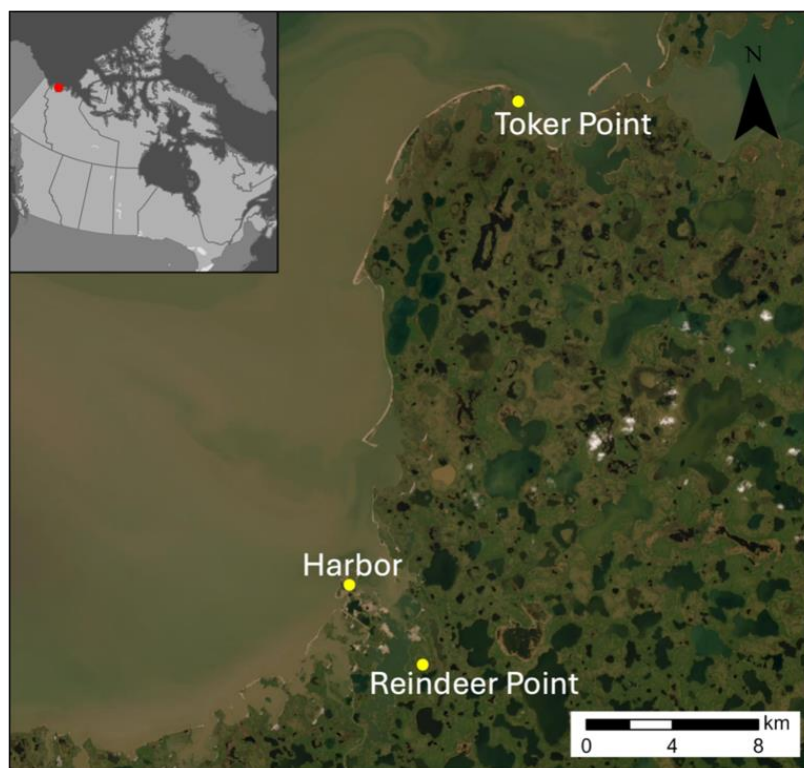
104 of rapid land retreat (Hynes et al., 2014; Lapham et al., 2020; Lim et al., 2020). Combined with sea level rise (Hill et  
105 al, 1993), it is projected that a substantial amount of terrestrial soil will become part of the ocean seafloor either by  
106 erosion and deposition or by subsidence of land and submersion. Over the past 15 years, extensive studies on  
107 Tuktoyaktuk's coastal environment, driven by the region's vulnerability to climate change, highlighted challenges for  
108 the Inuvialuit population relying on hunting, fishing, trapping and harvesting (Andrachuk and Smit, 2012).

109 Active layer samples were collected from two sites: an inland site, Reindeer Point (RP) and a coastal site, Toker Point  
110 (TP). Talik sediments were also collected at both RP and TP sites from polygonal troughs and pondlets and sediments  
111 from a marine site, Harbor, completed the transect from terrestrial to marine settings. RP was selected as the inland  
112 site because it features a polygonal patterned ground typical of the region, and is located in a stable region not directly  
113 affected by coastal processes such as storm surges, tides, seawater intrusion, erosion etc. The thermokarst lake margin,  
114 about 300m south of RP has remain unchanged since aerial photos began recording the evolution of the landscape in  
115 1947 (Fig S1). TP was selected as the coastal site because of the strong coastal processes such as tides and storm surge  
116 that regularly lead to seawater intrusion in this polygonal patterned ground, strongly influenced by ground subsidence.  
117 The Harbor site was selected about 400 m offshore in the Harbor of Tuktoyaktuk where total water depth was 20 m  
118 and cold marine bottom waters were overlain by a 10 m surface brackish water layer. 25 cm sediment cores were  
119 collected using a UWITEC gravity corer. The sediments consisted of recently deposited silty sands originating from  
120 the strong erosional processes occurring in the region (Whalen et al., 2022). The site was accessible by small  
121 watercraft. At RP and TP sites, soil profiles were extracted from the active layer by digging a soil pit with a shovel.  
122 To retain an intact stratigraphic relationship, samples were taken from the wall of the soil pit. Biogenic ebullition  
123 gases were collected from pondlets at RP and TP. Pondlets were located within sampled polygonal patterned ground  
124 and are defined as small (1 to 3 m<sup>2</sup>) and shallow standing bodies of water, potentially draining seasonally. Samples  
125 were trapped using a plastic funnel attached to a 20 mL glass vial. Surface soil lying at the bottom of the pondlets  
126 (Fig. 1) were poked until the vial was filled with gas. Once full, vials were crimped with 20 mm butyl rubber stoppers  
127 and aluminum caps. Samples were kept frozen until the time of analyses.



129 **Figure 1.** Schematic representation of polygonal tundra with peat accumulation as seen in continuous permafrost  
130 environments and sampling design for this study. High-centered polygons are associated with drier conditions, while  
131 low-centered polygons, troughs and pondlets are associated with humid or water-saturated conditions. Vegetation  
132 cover and OM reflect the hydrology of sites. Not to scale.

133



134

135 **Figure 2.** Map of study area indicating the sampled sites with yellow dots (ESRI, 2022). Harbor site is located in the  
136 marine waters of Tuktoyaktuk, Toker Point site is located in the coastal (intertidal) zone and Reindeer Point site is  
137 located inland. High resolution satellite imagery and pictures of soil profiles for RP and TP sites available in  
138 supplementary materials (Fig. S3).

139

140 The inland site, (RP), was located 750 m from the coast and 2 km East of Tuktoyaktuk in a polygonal  
141 patterned ground. This patterned ground is located in a depression, surrounded by elevated plateaus with observable  
142 ground water flowing into the valley. In this area, low-centered polygons exhibited higher moisture levels compared  
143 to high-centered polygons. High-centered polygons were colonized by shrubs and small flowering plants like  
144 *Ericaceae*, while low-centered polygons were dominated by hydrophilic plants such as grasses and sedges. Wet  
145 troughs delimited the polygons, with vegetation reflecting waterlogged conditions. The mean active layer and talik  
146 thickness across RP was about 35 cm. Profile 10A was collected from a trough and presented water-saturated  
147 conditions with brown OM. Profiles 10B and 10D were collected from high-centered polygons and characterized by  
148 unsaturated conditions with dark brown OM and presence of roots until 20 cm depth. Profile 10C was collected from

149 a low-centered polygon and consisted of reddish-brown peat throughout. Profiles 10A, 10B and 10D did not consist  
150 of peat.

151 The coastal site (TP) is located 20 km NW of Tuktoyaktuk, featuring a polygonal patterned ground, largely  
152 colonized by *Carex sp.*, a type of graminoid plant common near Arctic coastlines. The mean active layer and talik  
153 depths were 35 cm. The site's dynamics are influenced by the twice-daily ebb and flow of tides. Profile 07 was  
154 collected from a water-saturated low-centered polygon, located in the intertidal zone. The soil color was very dark  
155 greyish black. Profile 08 was collected from a water-saturated polygonal trough not immediately located in the  
156 intertidal zone, but which floods during storms. The soil was characterized by dark greyish-brown OM mixed with  
157 sand. Finally, profile 09, was collected from the center of a higher-centered polygon situated in the middle intertidal  
158 zone. The active layer appeared water unsaturated. The soil from this site consisted of a mixture of black organic-rich  
159 material and sand. The sand found in samples from TP appeared to be wind-deposited from nearby dunes.

## 160 **2.2 Sulfates and chloride concentrations in sediments**

161 The extraction of sulfate and chloride from sediments and soils pore-water was conducted through a leaching  
162 experiment following Lacelle (2019). Frozen aliquots of sediments and soils were thawed at 4°C overnight, then  
163 weighed, dried in the oven at 60°C for 24 hours and re-weighed to determine the densities. Aliquots of dried material  
164 were put in 50 mL falcon tubes with nanopure water following a 1:10 ratio. Tubes were then shaken for one hour to  
165 promote leaching of anions towards the aqueous phase of the solution. Once the leaching process was done, 2 mL of  
166 the aqueous solution was filtered using 0.2 µm pore size Whatman 25 mm GD/X syringe filters and transferred in  
167 disposable microtubes. Concentrations of sulfate and chloride were measured by ion chromatography using a Thermo  
168 Dionex Integriion at UQAR's Chemistry department facilities with a limit of detection of 0,01 µg/mL. The measured  
169 concentrations are expressed in mmol g<sup>-1</sup> wet-weight<sup>-1</sup> of material (mmol g<sup>-1</sup> wweight<sup>-1</sup>). Only one measurement per  
170 sample was performed as stability tests revealed variability of less than 3% between measured samples. The error on  
171 each value was calculated by the least squares method (Skoog et al., 2014).

## 172 **2.3 Methane production rates in incubations**

173 Long-term sediment and soil incubations under anoxic conditions were used to assess CH<sub>4</sub> production rates  
174 over several months by measuring CH<sub>4</sub> accumulation in the vials' headspace. The objective was to simulate the  
175 increased connectivity between the land and the ocean in the coastal environment of the Canadian Arctic, which  
176 represents an important aspect of the ongoing regional environmental transition. Collected sediments and soil profiles  
177 were immediately sub-sampled based on depth, at 5 or 10 cm intervals, according to shifts in sedimentary units. To  
178 prepare incubations, about 4 mL of sediment and exactly 2 mL of brackish water (collected from the coast) were  
179 immediately transferred into 20 mL glass vials. Incubation vials were crimped with 20 mm blue chlorobutyl rubber  
180 stoppers and aluminum caps. The bottles were flushed with nitrogen gas (Alpha Gaz 1) at a rate of 300mL/min for 2  
181 minutes in the field to replace the air with a nitrogen atmosphere. Four incubations were prepared for each sampled  
182 depth; 3 were kept for measurements of CH<sub>4</sub> production rates (triplicates) and one served for isotopic analyses.  
183 Incubations were kept at a constant temperature of 4°C throughout the entire 339 days incubation period with no

184 fluctuations. Substrate concentrations were not actively controlled or monitored, aside from repeated measurements  
185 of headspace methane. For logistical reasons, we were not able to measure CH<sub>4</sub> concentrations from the incubations  
186 in the first few weeks and the last measurement was conducted at day 339. The brackish water added to all incubations  
187 contained  $5.7 \pm 0.0$  mmol g<sup>-1</sup> wweight<sup>-1</sup> of sulfate and  $28.7 \pm 0.5$  mmol g<sup>-1</sup> wweight<sup>-1</sup> of chloride.

188 Analyses of the CH<sub>4</sub> concentrations in the headspace of the vials were performed on a gas chromatograph  
189 (Agilent 8900) equipped with a flame ionization detector (GC-FID) at UQAR facilities. The GC-FID is equipped with  
190 a 100 μL injection loop to ensure a consistent volume of sample is analyzed. To saturate the injection loop, 300 μL  
191 are taken from the headspace of the vials and transferred to the injection loop with a gas-tight syringe. Prior to  
192 injection, samples were shaken for 30 seconds to equilibrate headspace and sediment gases. This procedure was done  
193 every two weeks for 16 weeks to measure CH<sub>4</sub> accumulation in the headspace. The resulting production rates were  
194 calculated from the linear accumulation measured during the incubation period, and values are expressed in nmol of  
195 CH<sub>4</sub> per cubic centimeters of wet material per day (nmol cm<sup>-3</sup> d<sup>-1</sup>). The density of the collected samples varied widely,  
196 with some being organic deposits and peat, while others contained higher mineral content. Consequently, the CH<sub>4</sub>  
197 production rates were expressed volumetrically to account for these discrepancies which are more representative of  
198 the volume they occupy in the soil, sedimentary columns and landscape. The limit of detection of the GC-FID is 0.3  
199 ppm and all samples had higher concentrations. Each value represents the mean of triplicate measurements and the  
200 reported uncertainty on the measurement is the standard deviation on triplicates.

201 To estimate the potential total active layer CH<sub>4</sub> production (T), the active layer production rates were  
202 vertically integrated to obtain the total CH<sub>4</sub> production of each profile. Values are reported in mmol m<sup>-2</sup> d<sup>-1</sup> and were  
203 calculated using eq. 1:

$$204 \quad T = \frac{1}{100} \sum_{i=1}^n P_i \cdot e_i \quad [mmol m^{-2} d^{-1}] \quad \text{eq. 1}$$

205 Where  $P_i$  represents CH<sub>4</sub> production rate in layer  $i$  (nmol cm<sup>-3</sup> d<sup>-1</sup>),  $e_i$  represents the thickness of layer  $i$  (cm)  
206 and  $n$  represents the numbers of layers in the profile.

207 Using aerial imagery from 2022, the polygonal tundra at RP was mapped in QGIS, allowing for the  
208 discrimination between high-centered polygons, low-centered polygons and throughs (Fig S2). The total area of each  
209 geomorphological form was calculated based on the map data (Table S1). Landforms total areas were multiplied by  
210 the corresponding potential total active layer methane production (T) to estimate the total CH<sub>4</sub> produced in the  
211 polygonal tundra of RP over a day (mol d<sup>-1</sup>).

## 212 **2.4 Elemental and isotope composition of the sediment**

213 The total organic carbon (TOC) content of the sediments was measured by combustion using an elemental  
214 analyzer (ECS 8020, NC Technologies) combined with a gas chromatograph equipped with a thermal conductivity  
215 detector at ULaval facilities (The International Research Laboratory Takuvik). A 100 mg aliquot of sediment was  
216 thawed and weighed for each sample. They were then dried in an oven at 60°C for 48 hours and re-weighed to

217 determine their water content. Sediments were then ground using a granite mortar pestle and homogenized using a  
218 1.18 mm pore size sieve to remove roots and rootlets. Instruments were cleaned with ethanol between manipulations.  
219 Inorganic carbon was removed from sediments by adding 2.2 mL of 12M HCl in every sample. After reacting for 24  
220 hours, around 8 mg was encapsulated in tin foil capsules. Samples were kept in a desiccator until analyses. Values are  
221 expressed as % of carbon contained in the weighed sample (wt. %).

222 The organic carbon ( $\delta^{13}\text{C}$ -TOC) isotopic compositions were measured at UOttawa facilities (Jàn Veizer  
223 Stable Isotope Laboratory) using EA-IRMS (Delta Advantage, Thermo Germany). The sample preparation method  
224 was the same used for elemental analyses.  $\delta^{13}\text{C}$ -TOC values are denoted as  $\delta\text{‰}=10^3 \left( \frac{R_{\text{sample}}}{R_{\text{standard}}} - 1 \right)$ , where R is  
225  $^{13}\text{C}/^{12}\text{C}$  and standards refer to the Vienna Pee Dee Belmnite (VPDP).

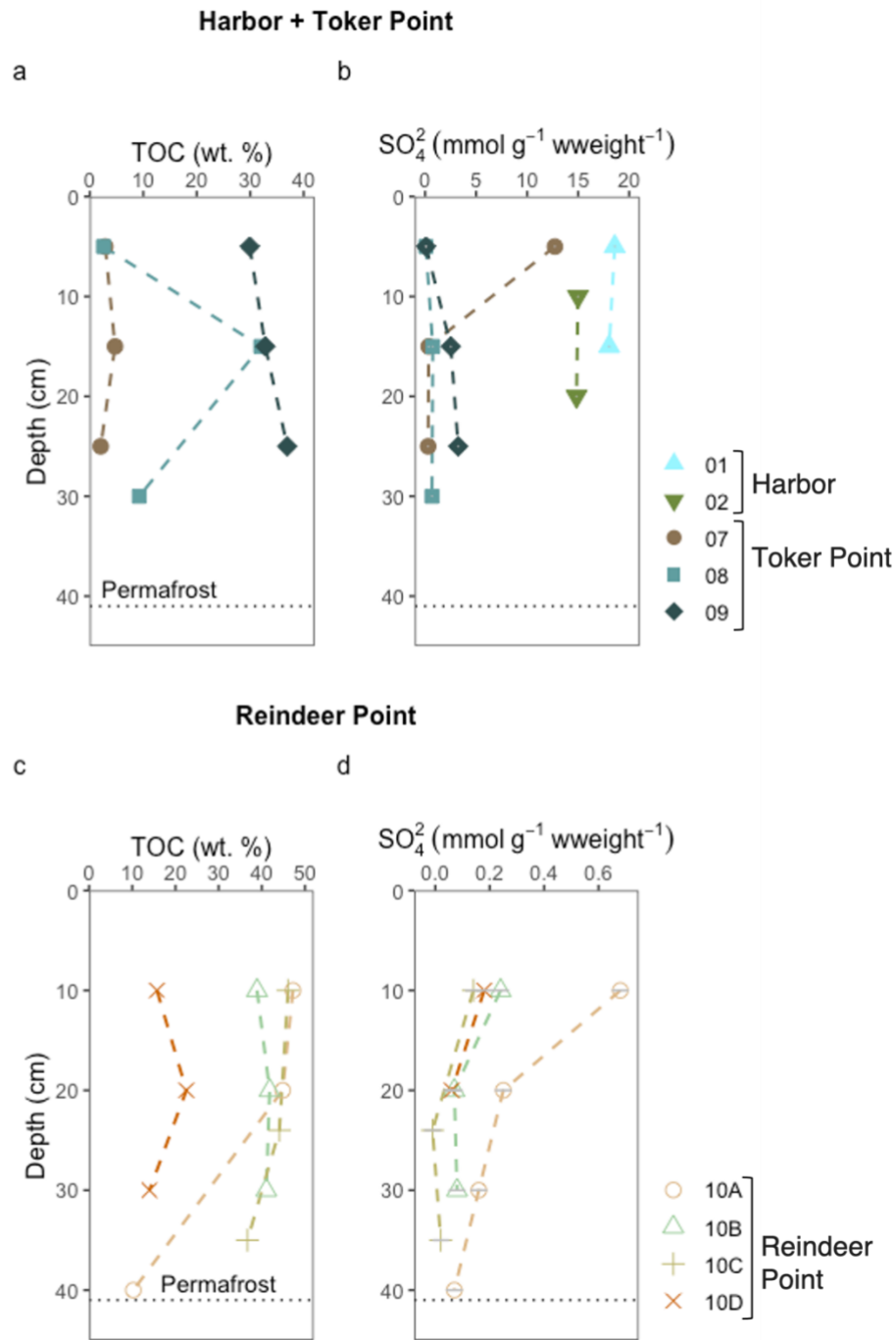
## 226 **2.5 Stable carbon isotopic composition of methane**

227 One incubation vial was analyzed for stable carbon isotopic composition of headspace methane ( $\delta^{13}\text{C}$ -CH<sub>4</sub>).  
228 Stable carbon from methane ebullition samples collected from pondlets were also analyzed. Both types of samples  
229 were analyzed with a cavity ring-down spectrometer (PICARRO G2201-i isotopic CO<sub>2</sub>/CH<sub>4</sub>) equipped with a 16-port  
230 distribution manifold and small sample introduction module (SSIM) at McGill (McGill Isotope Biogeochemistry  
231 Laboratory). Incubations were kept at 4°C in the dark for 8 months to let the microbial community stabilize and  
232 produce sufficient CH<sub>4</sub> for analysis. To stay in the detection range of the analyzer (1.8-1000 ppm CH<sub>4</sub>), a small volume  
233 of the headspace, proportional to CH<sub>4</sub> concentration in sample, was drawn from the incubation vial (0.2-6 mL). The  
234 sample was introduced to the 16-port manifold with a 21G needle connected to a disposable luer lock plastic syringe.  
235 Samples were diluted with zero air by the SSIM to reach a volume of 20 mL. Two or three measurements per sample  
236 were conducted depending on headspace concentration. Ebullition gases samples were analyzed following the same  
237 method. Measured values were corrected with internal certified methane standards (-59 ‰ and -42‰) from AirLiquide  
238 and stability of the analyzer was tested with injections of ambient air. Measured values were more precise than  $\pm$   
239 1.2‰. All  $\delta^{13}\text{C}$ -CH<sub>4</sub> values are expressed relatively to VPDB. While those isotopic analyses results provide valuable  
240 insight into methane cycling processes, they should be interpreted with caution in the absence of biological replication.

## 241 **3 Results**

### 242 **3.1 Soil description and composition**

243 TOC content in the sampled soils ranged from 2 to 47 wt. %, with no clear trend in relation to depth (Fig 3,  
244 a, c). The RP polygonal patterned ground featured organic soils with TOC content ranging from 14 to 47 wt. % (Fig  
245 3, c). The TP coastal polygonal patterned ground also featured organic soils with TOC content ranging from 2 to 37  
246 wt. % (Fig 3, a).



247

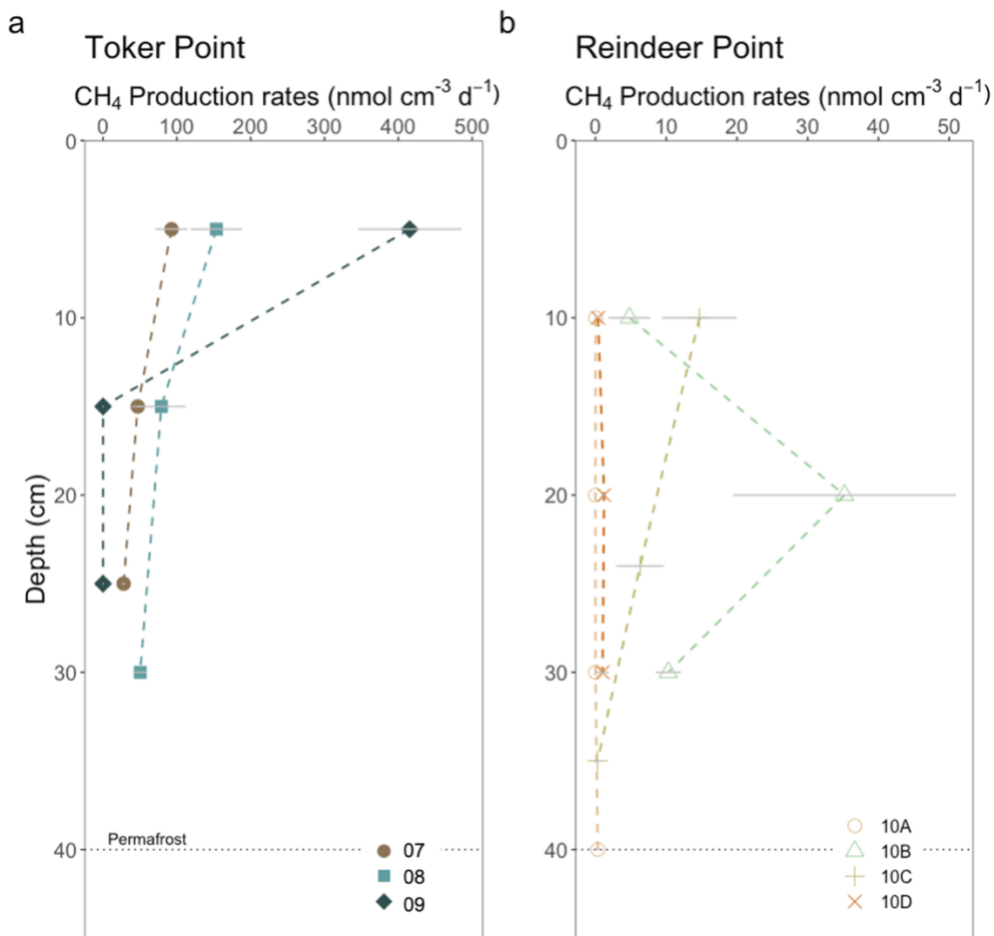
248 **Figure 3.** Total organic carbon and sulfate ( $\text{SO}_4^{2-}$ ) concentrations in sediment or soil of different sites in this study.  
 249 The datasets are separated into two for clarity. The upper part of the figure (panels A and B) displays the data of the  
 250 marine site Harbor (profile 01 and 02), and the coastal site, Toker Point (profile 07, 08 and 09). The lower part of the  
 251 figure (panel C and D) displays the data from the inland site Reindeer Point (profile 10A, 10B, 10C and 10D). The  
 252 black horizontal dotted line in each graph represents the permafrost-active layer or talik interface except for the Harbor

253 site, where the talik is much deeper but not measured. TOC data from Harbor site is not available. A uniform color  
254 pattern is used throughout this manuscript.

255 RP, the inland site, had low sulfate and chloride concentrations relative to TP, the coastal site (Fig 3 (b), (d)  
256 and S2). Sulfates at RP ranged from null concentrations to  $0.68 \pm 0.03 \text{ mmol g}^{-1} \text{ wweight}^{-1}$ , while at TP, profiles  
257 exhibited varying concentrations and patterns in relation to depth. Sulfate concentrations, ranged from  $0.07 \pm 0.03$  to  
258  $12.72 \pm 0.03 \text{ mmol g}^{-1} \text{ wweight}^{-1}$ . Profile 07, the low-centered polygon, exhibited the highest sulfates concentrations  
259 of all TP site at its surface ( $12.72 \pm 0.03 \text{ mmol g}^{-1} \text{ wweight}^{-1}$ ), with concentrations decreasing drastically with depth,  
260 reaching  $0.29 \pm 0.03 \text{ mmol g}^{-1} \text{ wweight}^{-1}$  at 25 cm (Fig 3, a). In profile 09, the high-centered polygon, sulfate  
261 concentrations increased with depth ranging from  $0.09 \pm 0.03 \text{ mmol g}^{-1} \text{ wweight}^{-1}$  at 5 cm to  $3.2 \pm 0.03 \text{ mmol g}^{-1}$   
262  $\text{wweight}^{-1}$  at 25 cm. Finally, profile 08, characterized as a polygonal trough, had sulfate concentrations ranging from  
263  $0.07 \pm 0.03$  to  $0.75 \pm 0.03 \text{ mmol g}^{-1} \text{ wweight}^{-1}$ . The highest sulfate concentrations measured in this study were found  
264 in the sediments of the Harbor site, with a mean value of  $16.6 \text{ mmol g}^{-1} \text{ wweight}^{-1}$  (Fig 3, a).

### 265 3.2 Methane production

266 Rates of  $\text{CH}_4$  production in incubations of sediment and soil with brackish water were undertaken at the three  
267 studied sites: RP, TP and Harbor. Production rates ranged from null to  $415.4 \pm 69.2 \text{ nmol cm}^{-3} \text{ d}^{-1}$  (Fig 4) throughout  
268 all samples in this study. At RP, the maximum  $\text{CH}_4$  production rate of  $35.2 \pm 15.7 \text{ nmol cm}^{-3} \text{ d}^{-1}$  was measured in the  
269 trough profile (10B) at a depth of 20 cm. Lower values were obtained for the surface and at the talik-permafrost  
270 interface. The low-centered polygon (10C) had its maximum  $\text{CH}_4$  production rate in the surface, decreasing with  
271 depth. High-centered polygons (10A and 10D) had very low production rates along their depth profiles ranging  
272 between null to  $1.2 \pm 0.2 \text{ nmol cm}^{-3} \text{ d}^{-1}$ . Both water-saturated trough and low-centered polygon (10B,10C) had  
273 relatively high  $\text{CH}_4$  production rate compared with the high-centered polygon profiles (10A, 10D), which were water-  
274 unsaturated.

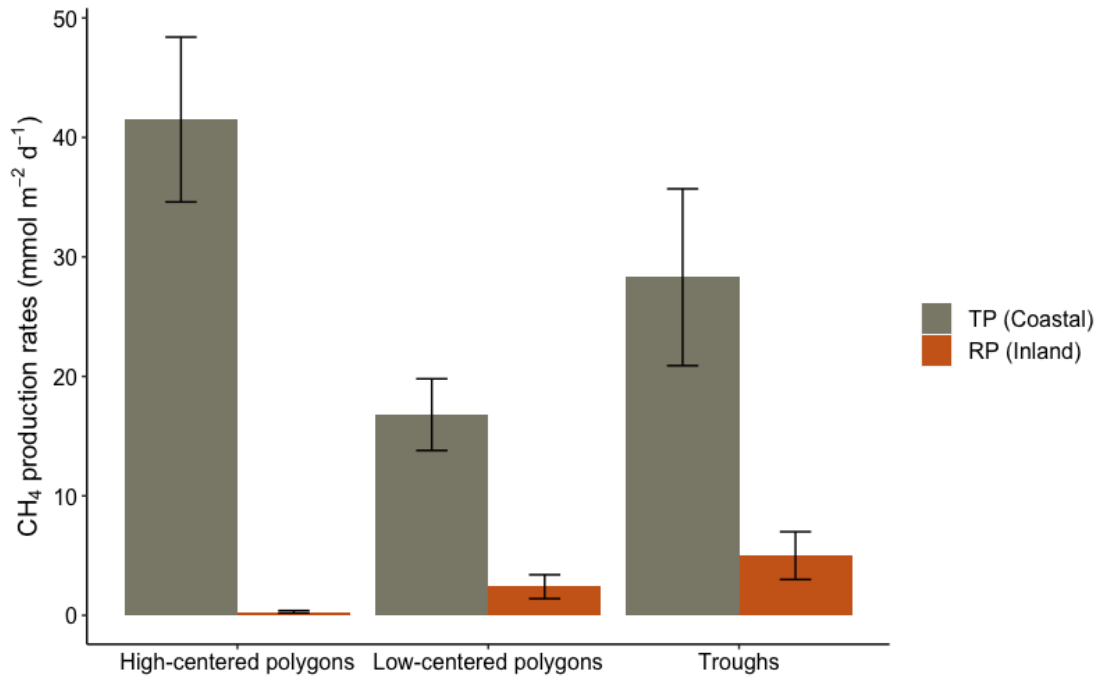


275

276 **Figure 4.** CH<sub>4</sub> production in incubations of soil and sediment with brackish water from (a) TP and (b) RP. Each  
 277 datapoint represent the mean value of three incubations. The error bars in grey lines are equal to the standard deviation  
 278 of the three separate incubations. Each profile corresponds to a specific landform. At Toker Point (panel A), profile  
 279 07 is from a low-centered polygon, profile 08 is from a trough and profile 09 is from a high-centered polygon. At  
 280 Reindeer point (panel B), profile 10A is from a high-centered polygon, profile 10B is from a trough, profile 10C is  
 281 from a low-centered polygon and profile 10D is from a high-centered polygon.

282 At TP, a maximum CH<sub>4</sub> production rate was recorded in profile 09, the high-centered polygon at  $415.4 \pm$   
 283  $69.2 \text{ nmol cm}^{-3} \text{ d}^{-1}$  at the uppermost depth but it quickly decreased in the subsurface. Profile 08, the trough, and profile  
 284 07, the low-centered polygon, had lower sub-surface CH<sub>4</sub> production rates, but rates decreased less drastically with  
 285 depth with values being relatively high at the permafrost-talik and permafrost-active layer interface, respectively.  
 286 Profile 07 had values ranging from  $27.9 \pm 1.5 \text{ nmol cm}^{-3} \text{ d}^{-1}$  to  $92.8 \pm 21.2 \text{ nmol cm}^{-3} \text{ d}^{-1}$  and profile 08 had values  
 287 ranging from  $50.4 \pm 7.2 \text{ nmol cm}^{-3} \text{ d}^{-1}$  and  $153.7 \pm 33.9 \text{ nmol cm}^{-3} \text{ d}^{-1}$  (Fig 4). In general, at TP, the coastal site, much  
 288 higher CH<sub>4</sub> production rates were measured than at RP, the inland site (Fig 4). The mean CH<sub>4</sub> production rate measured  
 289 at RP was  $5.7 \text{ nmol cm}^{-3} \text{ d}^{-1}$ , while at TP it was  $96.2 \text{ nmol cm}^{-3} \text{ d}^{-1}$ . The incubations with silty-clay Harbor sediments  
 290 did not have measurable CH<sub>4</sub> production rates (Fig S5).

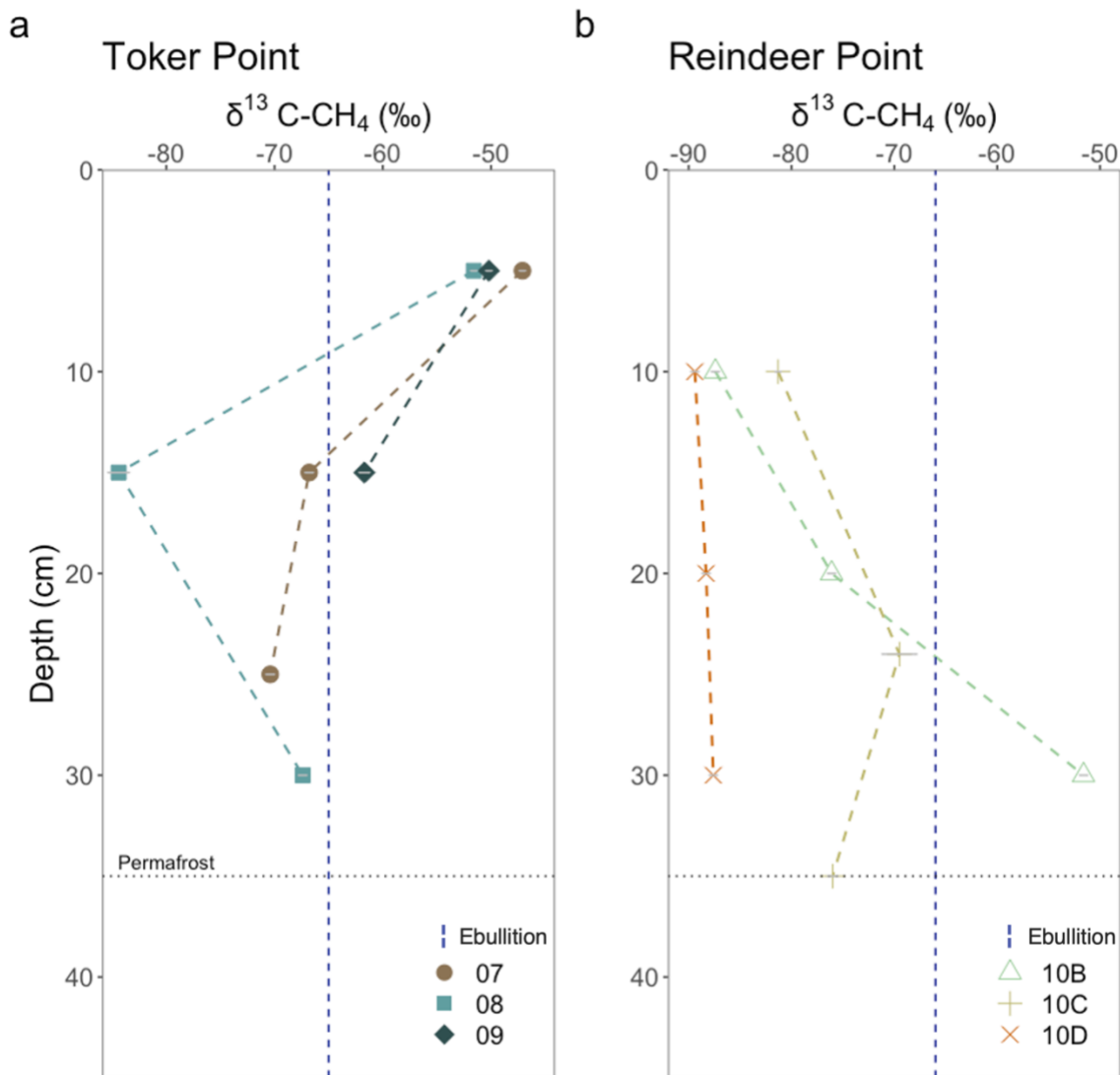
291 Estimated total CH<sub>4</sub> production rates were calculated for each geomorphological landforms of RP and TP  
 292 sites. At RP, the total CH<sub>4</sub> production estimated for the high-centered polygons (profile 10A and 10D), low-centered  
 293 polygon (profile 10C) and trough (profile 10B) were  $0.3 \pm 0.1 \text{ mmol m}^{-2} \text{ d}^{-1}$ ,  $2.4 \pm 1.0 \text{ mmol m}^{-2} \text{ d}^{-1}$  and  $5 \pm 2 \text{ mmol}$   
 294  $\text{m}^{-2} \text{ d}^{-1}$ , respectively (Fig 5). At TP, the total CH<sub>4</sub> production estimated for the high-centered polygon (profile 09), the  
 295 low-centered polygon (profile 07) and the through (profile 08) were  $41.5 \pm 6.9 \text{ mmol m}^{-2} \text{ d}^{-1}$ ,  $16.8 \pm 3.0 \text{ mmol m}^{-2} \text{ d}^{-1}$   
 296 and  $28.3 \pm 7.4 \text{ mmol m}^{-2} \text{ d}^{-1}$ , respectively (Fig 5). In all landforms, the total CH<sub>4</sub> production rates were higher in the  
 297 coastal site, TP, than the inland site, RP.



298  
 299 **Figure 5.** Total CH<sub>4</sub> production rates (T) at Toker Point (Coastal) and Reindeer Point (Inland) organized by  
 300 geomorphological forms of high-centered polygons, low-centered polygons and troughs. High-centered polygons at  
 301 RP is the mean of two profiles. All other landforms at RP and TP are one profile. The uncertainty on T is propagated  
 302 from the uncertainty of individual CH<sub>4</sub> production rates, not averages from replicate sites.

### 303 3.3 Isotopic composition of <sup>13</sup>C-CH<sub>4</sub>

304 In parallel with CH<sub>4</sub> production rates, one incubation vial per depth was used to measure the stable carbon  
 305 isotopic composition of the CH<sub>4</sub> produced. At RP, the δ<sup>13</sup>C-CH<sub>4</sub> of the first sampled depth (10 cm) ranged from -  
 306 81.3‰ to -89.4‰. At TP, the coastal site, the δ<sup>13</sup>C-CH<sub>4</sub> signature of the first sampled depth (5 cm) ranged from -  
 307 47.1‰ and -51.6‰. The values cluster together based on site, suggesting surface OM degradation processes are most  
 308 similar within sites than between sites (Fig. 6). Profiles at RP became progressively enriched in <sup>13</sup>C with depth, except  
 309 for profile 10C where a more depleted value was observed at 35 cm. Conversely, at TP, profiles became depleted in  
 310 <sup>13</sup>C with depth, except for profile 08 where an enrichment was measured between 15 and 30 cm.



311

312 **Figure 6.** Isotopic composition of CH<sub>4</sub> produced in brackish water incubations from (a) TP and (b) RP. Each datapoint  
 313 corresponds to the mean value of two or three measurements done on one incubation, depending on the headspace  
 314 concentration. The dashed vertical lines correspond to in situ ebullition CH<sub>4</sub> collected in pondlets at each sampling  
 315 site (n=1). These values give information on the pathways used by the soil microbes to produce CH<sub>4</sub>. δ<sup>13</sup>C between -  
 316 65‰ and -50‰ is typically associated with acetoclastic methanogenesis, while δ<sup>13</sup>C between -110‰ and -60‰ is  
 317 associated with hydrogenotrophic methanogenesis (Hornibrook et al., 1997, 2000). The grey error bars on each point  
 318 represents the analytical uncertainty on the measured value. If not visible, the uncertainty is smaller than the point.

319 Ebullition samples from pondlets were also measured for stable isotopes. The ebullition samples represent  
 320 the net δ<sup>13</sup>C signature of methane produced in the sediments of pondlets at RP and TP. At RP, CH<sub>4</sub> ebullition from a  
 321 sampled thaw pond had a δ<sup>13</sup>C of -66.1‰ (fig 6). At TP, CH<sub>4</sub> ebullition from a sampled pondlet had a δ<sup>13</sup>C-CH<sub>4</sub> of -  
 322 65.0‰ (fig 6).

## 323 4 Discussion

### 324 4.1 Addition of brackish water to anoxic incubations did not strongly suppress methanogenesis

325 Before discussing the effects of brackish water addition in incubation experiments, it is important to clarify the  
326 role of sulfate measured in situ within soil and sediment profiles. Across the studied sites, sulfate concentrations varied  
327 with depth and between landforms; however, this spatial variability did not show a consistent relationship with  
328 methane production rates measured in the incubations (Fig S4). A few layers clearly contained higher sulfate amounts.  
329 However, layers characterized by higher or lower sulfate concentrations did not systematically correspond to lower or  
330 higher CH<sub>4</sub> production, indicating that in situ sulfate availability alone does not explain the observed patterns in  
331 methane production across profiles. This interpretation is subject to important limitations. Sulfate and chloride  
332 concentrations were measured at single points within each profile and were not replicated across multiple locations  
333 within the same landform, preventing resolution of fine-scale spatial heterogeneity in electron-acceptor availability.  
334 As a result, sulfate concentrations are interpreted here as first-order indicators of geochemical context rather than as  
335 spatially representative or mechanistic controls on methane production. Given these constraints, we focus the  
336 following discussion on the experimental addition of sulfate via brackish water during anoxic incubations, which  
337 evaluate how episodic marine influence may affect methane production potential in coastal permafrost environments.

338 Despite the addition of brackish water containing sulfate to incubations, the range of CH<sub>4</sub> production rates  
339 measured in this study is consistent with reports for anaerobic incubations of recently thawed permafrost soils,  
340 suggesting that the input of brackish water to some coastal systems may not inhibit CH<sub>4</sub> production. For example, in  
341 the talik of Big Trail Lake, a young thermokarst lake in the interior of Alaska, CH<sub>4</sub> production rates based on  
342 incubations ranged between 4.7 and 16.1 nmol cm<sup>-3</sup> d<sup>-1</sup> (Pellerin et al., 2022), while in incubations from Vault Lake,  
343 another thermokarst lake in the interior of Alaska, CH<sub>4</sub> production rates varied between 11.1 and 275 nmol cm<sup>-3</sup> d<sup>-1</sup>  
344 (Heslop et al., 2015). In active layer incubations from the Yamal Peninsula in NW Siberia (Russia), CH<sub>4</sub> production  
345 rates of incubations varied between 0.1 and 33.8 nmol cm<sup>-3</sup> d<sup>-1</sup> (Heyer et al., 2002). This indicates that overall, the  
346 CH<sub>4</sub> production rates measured at both TP and RP are within the range observed in typical ice-rich permafrost settings  
347 and reasonable for the environment studied (Fig. 4). We note that our experimental design did not include parallel  
348 incubations without brackish water or with sulfate concentration gradients; therefore, our interpretation relies in part  
349 on comparison with previous incubations of Tuktoyaktuk soils conducted without brackish water addition (Lapham  
350 et al., 2020) and should be regarded as exploratory rather than definitive. Lapham et al. (2021) conducted sediment  
351 incubation experiments using a core collected from the coast of the Tuktoyaktuk Peninsula. In their study, CH<sub>4</sub>  
352 production was measured under anaerobic conditions at 15 °C, without the addition of water, over a 35-day period.  
353 The reported CH<sub>4</sub> production rate was 0.07 nmol cm<sup>-3</sup> d<sup>-1</sup>. Although their incubations were performed over a shorter  
354 duration and at a significantly higher temperature than those in the present study, the measured rate reflects CH<sub>4</sub>  
355 production under relatively natural, unamended conditions. This value is comparable to the lowest CH<sub>4</sub> production  
356 rates measured in our incubations at both the coastal (TP) and inland (RP) sites and provides a useful reference for  
357 CH<sub>4</sub> production under unamended conditions.

358 The novel aspect of this study is that it attempts to understand marine influence on OM degradation by addition  
359 of brackish water to sediment and soil incubations of a fully marine site (Harbor), one that is periodically submerged  
360 (TP) and never submerged (RP). This simulates the input of seawater to the active layer and taliks of tundra soils (RP)  
361 as well as providing reference sites with a high marine influence (Harbor and TP). We hypothesized that the addition  
362 of locally obtained brackish water, which contained sulfate (5.7 mmol L<sup>-1</sup>), to the incubations, would suppress CH<sub>4</sub>  
363 production in RP, the inland site and potentially also at TP, the coastal site. This reasoning is because supplying sulfate  
364 to low sulfate organic-rich sediment would promote sulfate reduction, which is thermodynamically more favorable  
365 than methanogenesis, thereby competitively inhibiting it (Lovely and Klug, 1983; Oremland and Polcin, 1982). This  
366 hypothesis is also consistent with field observations; organic matter mineralization in brackish wetlands is consistently  
367 dominated by bacterial sulfate reduction (Bridgham et al., 2013; Torres-Alvarado et al., 2005) where little to no  
368 CH<sub>4</sub> emissions are observed (Pönisch et al., 2022; Petersen et al., 2023; Kroeger et al., 2017). However, recent field  
369 studies show that in coastal permafrost soils, inundation and low sulfate concentrations do not necessarily suppress  
370 methanogenesis (Jenrich et al., 2025; Jenrich et al., 2024; Yang et al., 2023). These contrasting observations reveal a  
371 key knowledge gap in how marine influence controls carbon mineralization pathways in permafrost systems. By  
372 experimentally testing brackish water additions across sites with contrasting marine exposure, our study provides new  
373 mechanistic insight into the regulation of OM degradation and CH<sub>4</sub> production under ongoing Arctic coastal change.

374 RP had low sulfate concentrations before addition of the brackish water but so did many of the profiles from TP  
375 (Fig 3). In the Harbor sediments, no methane production was observed (Fig S5). This is consistent with the competitive  
376 inhibition of methanogenesis by energetically favorable redox reactions with electron acceptors like oxygen, nitrate,  
377 iron oxides or sulfate that is typical of marine systems e.g. (Martens and Berner, 1974) as well as the potential for  
378 anaerobic oxidation of methane (AOM). Given that the Harbor sediments already had high sulfate concentrations, the  
379 lack of methane production with addition of brackish water was expected. However, strong CH<sub>4</sub> production was  
380 observed in the incubations of both the coastal site TP and the inland site RP, indicating that CH<sub>4</sub> production was not  
381 halted by the addition of sulfate via the brackish water addition at those sites. While sulfate reduction rates were not  
382 measured and therefore not demonstrated directly in our incubations, a strong sulfide smell was recorded when  
383 opening most of the incubations at the end of the experiment. This observation may indicate the coexistence of sulfate  
384 reduction and methanogenesis during the incubations. However, to rigorously assess this observation, future studies  
385 should include tracer-based sulfate reduction assays and microbial functional gene analysis.

386 Coexistence of sulfate and methanogenesis within complex sediment systems such as estuarine, coastal and salt  
387 marsh sediments, as well as thermokarst lasens has been widely reported (Lovely et al., 1982; Oremland and Taylor,  
388 1978; Sela-Adler et al., 2017; Yang et al., 2023). Two main mechanisms are invoked to explain this co-existence in  
389 our incubation experiment: (1) noncompetitive methanogenesis (i.e. methylotrophic methanogenesis) and (2)  
390 syntrophic methanogenesis. (1) Noncompetitive substrates are substrates like methanol and methylamines that are  
391 used by methanogens alone and cannot be used with electron acceptors like sulfate (Lovley and Klug, 1983; Oremland  
392 et al., 1982). Noncompetitive substrates are thus microbially converted to CH<sub>4</sub>, even in sediments with high sulfate  
393 concentrations (Maltby et al., 2018; Yuan et al., 2019). For example, in salt marshes, where high sulfate concentrations

394 are often found, elevated CH<sub>4</sub> emissions are suggested to mainly stem from noncompetitive methanogenesis (Comer-  
395 Warner et al., 2022; Poffenbarger et al., 2011; Yuan et al., 2019). In the sulfate reducing zone of sediments from the  
396 Baltic Sea, where ample sulfate is found in the porewaters, seasonal methanogenesis rates were measured up to 1.3  
397 nmol cm<sup>-3</sup> d<sup>-1</sup> due to noncompetitive substrates (Maltby et al., 2018). In permafrost soils, methanol, methylamines  
398 and the microorganisms capable of degrading them have been observed but their concentrations are typically low  
399 (Coolen and Orsi, 2015; Kramshoj et al., 2018). However, our study sites are on a coast undergoing a rapid  
400 transgression which may be driving imbalances between substrate supply and microbial abundances. The rates of  
401 methane production observed at RP and TP of up to 154 nmol cm<sup>-3</sup> d<sup>-1</sup> contrast with reported values for  
402 methylotrophic methanogenesis (Maltby et al., 2018). Based on these numbers, noncompetitive substrates likely play  
403 a small role in the total methane production at our study sites but further investigation into methylotrophic methane  
404 production in coastal environments will allow to document the overall role of methylotrophic methane production in  
405 coastal permafrost settings.

406 (2) Syntrophic methanogenesis occurs when molecular hydrogen produced by acetoclastic sulfate-reducing  
407 bacteria is used by hydrogenotrophic methanogens. In this syntrophy, the chemical energy is shared via interspecies  
408 hydrogen transfer (Ozuolmez et al., 2015). For instance, in permafrost soils of Sweden, it was demonstrated that  
409 syntrophic methanogenesis was favored in anoxic and water-saturated soils by an elevated abundance in methanogens  
410 and their syntrophic partners (Keuschnig et al., 2022). As the incubation experiment in our study at RP and TP featured  
411 water-saturated and anoxic environments, syntrophic methanogenesis could participate in the co-occurrence of sulfate-  
412 reduction and methanogenesis. This mechanism is consistent with most incubations producing methane with a  $\delta^{13}\text{C}$   
413 value in the range of hydrogenotrophic methanogenesis (see below).

414 Measuring methane production through incubations inherently has limitations as they prevent continuous inputs  
415 of microorganisms, fresh OM and nutrients that would occur in the natural environment. This can create a “bottle  
416 effect”, which leads to restrictions in microbial community composition, limits the input of nutrients and leads to the  
417 accumulation of metabolites which would normally be degraded (Ionescu et al., 2015). Typically, overestimation of  
418 microbial processes rates is observed compared to *in situ* data (Sherr et al., 1999). The overestimation of CH<sub>4</sub>  
419 production rates by incubations relative to the *in situ* rates are difficult to assess because of a lack of data in permafrost  
420 environments (Heslop et al., 2020). Furthermore, a lag time between the start of anaerobic incubations and maximum  
421 CH<sub>4</sub> production rate is widely documented, which appears to be the case for both active layer and thawed permafrost  
422 incubations (Holm et al., 2020; Knoblauch et al., 2018; Knoblauch et al., 2013; Roy Chowdry et al., 2015). Drier or  
423 water-unsaturated conditions lead to a longer lag time before the onset of maximum CH<sub>4</sub> production (Treat et al.,  
424 2015). Microbial community composition in the soil or sediment also exerts a strong control on the organic carbon  
425 degradation and has been shown to change throughout the incubations (Holm et al., 2020). Low initial methanogen  
426 population in soils can contribute to this lag time, but other factors such as disturbance of sediment during sampling,  
427 substrate availability and redox state can also contribute to the observed lag time in some incubations (Treat et al.,  
428 2015; Roy Chowdry et al., 2015).

429 Furthermore, it is also possible that a “priming effect” from the addition of brackish water in incubations could  
430 have supercharged OM degradation with marine organic carbon, nutrients and microorganisms (Bianchi, 2011), which  
431 may have enhanced CH<sub>4</sub> production. However, this priming effect was not observed in the Harbor sediments which  
432 were amended with the same brackish water. Furthermore, CH<sub>4</sub> ebullition samples collected from pondlets adjacent  
433 to RP and TP exhibited broadly similar δ<sup>13</sup>C values to methane produced in incubations (Fig 6), suggesting a similitude  
434 in microbial degradation pathways to methane *in situ* and in the incubations. Despite these uncertainties, our dataset  
435 shows clear depth trends and landscape-level variations, indicating that even under brackish water addition, local  
436 conditions will strongly influence CH<sub>4</sub> production.

#### 437 **4.2 CH<sub>4</sub> production pathways depend on hydrology and organic matter lability**

438 The addition of brackish water resulted in incubation conditions being water-saturated in all cases, but it  
439 appears that biological and hydrological conditions of the polygonal patterned grounds influenced the magnitude of  
440 CH<sub>4</sub> production, nonetheless.

441 In all landforms, CH<sub>4</sub> production rates were lower at the inland site, RP than at TP, the coastal site (Fig 4).  
442 Inland, low-centered polygons and troughs have typically higher CH<sub>4</sub> fluxes than unsaturated landforms like high-  
443 centered polygons (Roy Chowdry et al., 2015; Martin et al., 2018; Zheng et al., 2018) which indicates they may also  
444 have higher CH<sub>4</sub> production rates. Within sites in our study, brackish water amended incubations of high-centered  
445 polygon soils had lower CH<sub>4</sub> production rates, while brackish water amended incubations of troughs and low-centered  
446 polygons had higher CH<sub>4</sub> production rates (Fig 4). This indicates that for the degradation of organic matter into CH<sub>4</sub>  
447 in tundra soils, increasing seawater interactions through coastal processes, such as submersion due to subsidence or  
448 increased storm severity, resulting in the input of seawater in terrestrial soils, does not halt CH<sub>4</sub> production. It also  
449 shows that landforms and local hydrology remain important in controlling the microbial communities which affects  
450 the resulting CH<sub>4</sub> production. Differences among landforms and sites are generally large and clearly exceed the range  
451 of variability as shown by the uncertainty, supporting the use of means with standard deviations to convey contrasts  
452 without formal statistical tests. This approach allows us to highlight pronounced differences in methane production  
453 potential and geochemical context across coastal and inland sites.

454 Marine OM and nutrient inputs from tides and storm surges may contribute to the higher lability of OM and  
455 could fuel greater fermentation (Valdemarsen and Kristensen, 2010). It was reported that 8.7% of the organic carbon  
456 in nearshore sediments of Herschel Island, Beaufort Sea, came from marine sources (Couture et al., 2018). This is  
457 relevant for the TP site because while δ<sup>13</sup>C signature of soils showed that terrestrial OM is dominant (Fig S6), marine  
458 OM may get transported and deposited in coastal soils during high tides and storm surges. Although our analyses  
459 could not detect the presence of marine OM in TP soils, the higher CH<sub>4</sub> production rates recorded in the incubations  
460 of TP, relatively to those of RP could in part be explained by marine OM and nutrient inputs. Interestingly, the high-  
461 centered polygon at TP, profile 09 (Fig 4), did not behave in a predictable manner, since it had very high CH<sub>4</sub>  
462 production rates on the surface. This elevated methane production rate coincided with the presence of substantial  
463 goose fecal deposits at TP, profile 09. While this observation suggests a potential local input of labile organic matter

464 and nutrients (e.g., N and P) and possibly a distinct surface microbial community, no direct measurements were  
465 conducted to establish a mechanistic link. This site-specific observation is therefore reported as contextual field  
466 information rather than evidence of causation. Lower in the profile, CH<sub>4</sub> production rates were very low, characteristic  
467 of the CH<sub>4</sub> production rates observed in water-unsaturated high-centered polygons (Fig 4). Therefore, in this instance,  
468 proximity with the coast may have influenced CH<sub>4</sub> production through the presence of fauna.

469 Stable carbon isotopic signature of CH<sub>4</sub> provides insights on the microbial processes involved in  
470 methanogenesis and on substrates used.  $\delta^{13}\text{C-CH}_4$  between -65‰ and -50‰ is typically associated with acetoclastic  
471 methanogenesis, while  $\delta^{13}\text{C-CH}_4$  between -110‰ and -60‰ is associated with hydrogenotrophic methanogenesis  
472 (Hornibrook et al., 1997, 2000). The stable isotopic signature of methylotrophic methanogenesis is between -83‰ and  
473 -72‰ (Penger et al., 2012), which overlaps with the hydrogenotrophic interval, precluding us from separating these  
474 two metabolic pathways. At RP, except for profile 10B,  $\delta^{13}\text{C-CH}_4$  had more negative values, consistent with the  
475 processing of recalcitrant organic matter through the hydrogenotrophic production pathway (Heffernan et al., 2022;  
476 Hodgkins et al., 2014). Profile 10B, a polygonal trough, had less negative  $\delta^{13}\text{C-CH}_4$  values more consistent with  
477 acetoclastic methanogenesis (Hornibrook et al., 1997). At TP, the coastal polygonal tundra,  $\delta^{13}\text{C-CH}_4$  at 5 cm depth  
478 is less negative, consistent with methanogenesis with more labile organic carbon and the acetoclastic production  
479 pathway (Hodgkins et al., 2014), transitioning to more negative values, associated to hydrogenotrophic production  
480 with depth. This shift suggests an input of labile OM in TP surface and sub-surface soils. This may be due to the labile  
481 OM from abundant geese fecal matter that was observed in the surface. It is also possible that *Carex sp.*, the dominant  
482 plant species of the site, may be a source of labile fermentation precursors (Galand et al., 2010; Liebner et al., 2015).  
483 To evaluate whether  $\delta^{13}\text{C-CH}_4$  covaried with other geochemical properties measured in this study,  $\delta^{13}\text{C-CH}_4$  values  
484 were examined alongside TOC content and sulfate concentrations; however, no consistent relationships were observed  
485 across landforms or depths (Fig. S4), indicating that methanogenic pathway signatures are not straightforwardly  
486 predicted by bulk TOC or sulfate availability at the scale investigated. However, it is clear that future work should  
487 integrate measurements of organic matter degradation, microbial community composition, and pore water chemistry  
488 to better resolve the mechanisms driving spatial variability in methane production.

#### 489 **4.3 Total CH<sub>4</sub> production rates are comparable to the net CH<sub>4</sub> fluxes measured in similar environments**

490 In a polygonal terrain of the Tuktoyaktuk Coastlands, net CH<sub>4</sub> fluxes from the center of high-centered polygons  
491 and troughs derived from flux chambers were measured to be  $1.9 \pm 20.4 \text{ mmol m}^{-2} \text{ d}^{-1}$  and  $13.0 \pm 20.4 \text{ mmol m}^{-2} \text{ d}^{-1}$   
492 respectively (Martin et al., 2018). These overlap with values of estimated total CH<sub>4</sub> production derived from the  
493 brackish water amended incubation experiments (Fig. 5). It is clear from the large variations in measured CH<sub>4</sub>  
494 emissions from the study of Martin et al., (2018) that incubations to estimate total active layer CH<sub>4</sub> production rates  
495 can discern small differences due to local variations that stem mostly from the polygonal features. For example, at  
496 RP a comparable polygonal terrain located in the same study area of Martin et al., (2018), the total CH<sub>4</sub> production of  
497 high-centered polygons and trough were  $0.3 \pm 0.1 \text{ mmol m}^{-2} \text{ d}^{-1}$  and  $5.0 \pm 2.0 \text{ mmol m}^{-2} \text{ d}^{-1}$  (Fig. 5), respectively which  
498 are significantly different. This indicates the role of polygonal forms in controlling the activity of microbial

499 communities which controls CH<sub>4</sub> production and the potential to scale more accurately CH<sub>4</sub> production at the  
500 landscape level based on landform distributions.

501 Interestingly, TP, the coastal site, had an estimated total CH<sub>4</sub> production rate comparable to emissions of a St.  
502 Lawrence estuary salt marsh which had a CH<sub>4</sub> flux of  $24 \pm 14.4 \text{ mmol m}^{-2} \text{ d}^{-1}$  (Comer-Warner et al., 2022). The St.  
503 Lawrence estuary salt marshes are affected by freeze-thaw cycles associated with seasons comparable to the freeze-  
504 thaw cycles observed in the active layer of Tuktoyaktuk coastlands despite lacking some characteristics features of  
505 our site like the presence of permafrost and rapid coastal erosion rates. CH<sub>4</sub> emissions and production within areas of  
506 coastal influence thus appear of similar magnitude. By comparison, mangrove forests, which are a major global source  
507 of CH<sub>4</sub> but a very different environment from coastal Arctic polygon terrain, had average CH<sub>4</sub> fluxes to the atmosphere  
508 of  $0.3 \pm 0.1 \text{ mmol m}^{-2} \text{ d}^{-1}$  (Rosentreter et al., 2018). In another study, the average measured CH<sub>4</sub> flux from a Yangtze  
509 Estuary (China) tidal salt marsh, with a subtropical monsoon climate, was  $2.4 \text{ mmol m}^{-2} \text{ d}^{-1}$  (Li et al., 2021). These  
510 reported values are similar to our study as well as other studies in the region. When considered alongside the global  
511 distribution of coastal wetlands, this similarity in flux magnitude becomes particularly relevant. Tropical coastal  
512 wetlands are dominated by mangroves (~147,000 km<sup>2</sup>), whereas Arctic wetlands cover approximately 3.5 million km<sup>2</sup>  
513 (Worthington et al., 2024). Even if only a small fraction of Arctic wetlands is located within coastal zones, their total  
514 extent is comparable to the global mangrove area (Worthington et al., 2024), suggesting that permafrost Arctic coastal  
515 wetlands could represent a non-negligible component of the global CH<sub>4</sub> budget and warrant further investigation.

516 The calculated total methane production rates (T) from TP and RP do not take into account aerobic and anaerobic  
517 oxidation of CH<sub>4</sub>, which will most likely reduce fluxes of CH<sub>4</sub> from these sites. Studies and models of Arctic soils  
518 emissions have highlighted that aerobic methanotrophy could consume more than half of the CH<sub>4</sub> produced in soils,  
519 greatly limiting surface emissions (Oh et al., 2020; Zheng et al., 2018). Furthermore, AOM has been shown to play  
520 an important role in attenuating CH<sub>4</sub> production in soils and sediments (Segarra et al., 2013; Winkel et al., 2019) but  
521 did not appear to influence significantly CH<sub>4</sub> production in incubations with thermokarst lake sediments (Lotem et al.,  
522 2023). While AOM represents a major sink for CH<sub>4</sub> in marine sediments (Knittel and Boetius, 2009; Reeburgh, 2007),  
523 the very different biogeochemical and hydrological characteristics of our coastal sites suggest that the role of AOM  
524 in these environments may diverge from that observed in fully marine systems. Recent work in coastal thermokarst  
525 lagoons, which can present key similarities to our coastal study sites due to episodic or persistent brackish water  
526 intrusion, have been shown to exhibit strong AOM control on CH<sub>4</sub> dynamics, particularly in sulfate-rich settings where  
527 AOM may constitute a major CH<sub>4</sub> sink (Yang et al., 2023). For the discussion of this study, we compared results of  
528 brackish water incubations to CH<sub>4</sub> emissions measured in other landscapes. Such comparisons provide valuable  
529 context by comparing long-term microbial production processes with net atmospheric fluxes. However, we emphasize  
530 that CH<sub>4</sub> production rates cannot be directly equated to CH<sub>4</sub> emissions.

531

532 **Table 1.** Total methane production in a context of brackish water addition in high-centered polygons, low-centered  
533 polygons and throughs during growing season applied to the spatial scale of the polygonal landscape of RP. Two

534 samples were taken for the high-centered polygon. The mean active layer and talik depth of the region is 35 cm. The  
535 error represents the propagation of the analytical uncertainty from the incubations results.

Geomorphological form	Relative area of each landform (km <sup>2</sup> )	Estimated Total CH <sub>4</sub> production (mol d <sup>-1</sup> )
High-centered polygons	0.0803	20.7 ± 10.3
Low-centered polygons	0.119	284 ± 123
Troughs	0.0362	182 ± 73.4

536

537 To better frame the potential impact of brackish water addition at scale, we extrapolated its consequence to a 25  
538 hectare area of polygonal tundra surrounding RP (Fig S2). This estimate simulates CH<sub>4</sub> production following the  
539 infiltration of brackish water into the terrestrial polygonal landscape around Tuktoyaktuk. This event could result from  
540 coastal flooding during storm surges, which are frequent in the Mackenzie River delta (Kokelj et al., 2012; Solomon  
541 et al., 2005). Taking into consideration the distribution of the polygonal features within RP and the relative areas of  
542 each landform, the CH<sub>4</sub> production rates in the active layer, excluding pondlets, for an area of 25 ha was calculated to  
543 be 487 mol d<sup>-1</sup> (Table 1) or 22 nmol m<sup>-2</sup> s<sup>-1</sup> and is consistent with the CH<sub>4</sub> emissions measured from various wetland  
544 types (Cui et al., 2024). The increasing sensitivity of wetlands to climate change and the preponderant role of carbon  
545 substrate availability in controlling global methane emissions (Hu et al., 2024) warrants further investigating CH<sub>4</sub>  
546 dynamics in thawing continuous permafrost landscapes and the role of coastal processes influencing these emissions.  
547 More polygonal tundra in various settings should be investigated as a comparison to the studied region. Further  
548 research on aerobic and anaerobic CH<sub>4</sub> oxidation is necessary to provide a more precise estimate of the CH<sub>4</sub> cycle  
549 inputs and outputs in a scope of the evaluation of its impacts on the greenhouse gas feedback loop.

## 550 **5 Conclusions**

551 The primary hypothesis for this study was that an increase in waterlogged environments due to coastal  
552 flooding and inundation processes would not enhance CH<sub>4</sub> production because of sulfate present in coastal waters.  
553 However, our incubation experiments revealed high CH<sub>4</sub> production rates in the presence of sulfates. Additionally,  
554 waterlogged conditions attributed to the ebb and flow of tides, seems to favor anoxic OM degradation and may  
555 potentially provide inputs of fresh OM and nutrients from marine sources, contributing to the elevated CH<sub>4</sub> production  
556 rates measured in the coastal setting of TP. Moreover, no conclusive explanation for the co-occurrence of sulfate-  
557 reduction and methanogenesis in our brackish water incubations was identified, but based on evidence, we suggest  
558 syntrophic methanogenesis could support this co-occurrence. More investigation on methylotrophic methanogenesis  
559 in coastal soils are needed as it can be an important process in saline environments (Conrad, 2020). Future studies  
560 should investigate CH<sub>4</sub> oxidation processes in greater detail, as they could provide crucial insights into Arctic coastal  
561 carbon cycling in sediments and soils affected by changing sea level.

562 **Data availability**

563 All raw data of incubation experiment and other analyses performed and generated by study are available as  
564 supplementary information.

565 **Competing interests**

566 The authors declare that they have no conflict of interest.

567 **Author contributions**

568 AP designed the experiment; ARL executed the experiments and analyses. AP, ARL, DW, RL participated in the  
569 fieldwork. PMJD provided lab space, equipment and insights for the stable carbon isotopes analyses on incubation  
570 CH<sub>4</sub>. RL performed all GIS analyses and maps. ARL performed the data interpretation and generated all figures. AP  
571 provided expertise on the writing and interpretation of figures. All authors reviewed and edited the manuscript.

572 **Acknowledgements**

573 We thank Santiago Mareque for assistance during field sampling. Mathieu Babin and Thi Hao Bui are acknowledged  
574 for assisting with the laboratory work performed at Université du Québec à Rimouski and at McGill University,  
575 respectively. Takuik Laboratory is acknowledged for providing analyses and results on  $\delta^{13}\text{C}$  and TOC content of  
576 sediments. We also thank the community of Tuktoyaktuk for providing wildlife monitors with insightful information  
577 on the territory during field sampling. This research was funded by NSERC Discovery Grant and Northern Supplement  
578 to AP. ARL acknowledges financial support from the NSERC Northern Scientific Training Program. PMJD  
579 acknowledges support from the NSERC Discovery Grant and the Canadian Foundation for Innovation.

580 **Financial support**

581 Support funds and grant agreement numbers are listed as specified upon manuscript registration.

582 **References**

583 AMAP: AMAP Climate Change Update 2019: An Update to Key Findings of Snow, Water, Ice and Permafrost in the  
584 Arctic (SWIPA) 2017, Arctic Monitoring and Assessment Programme (AMAP), Oslo, Norway, 12 pp., 2019.

585 AMAP: Snow, Water, Ice and Permafrost in the Arctic (SWIPA) 2017, Arctic Monitoring and Assessment Programme  
586 (AMAP), Oslo, Norway, xiv + 269 pp., 2017.

587 Andrachuk, M. and Smit, B.: Community-based vulnerability assessment of Tuktoyaktuk, NWT, Canada to  
588 environmental and socio-economic changes, *Regional Environmental Change*, 12, 867–  
589 885, <https://doi.org/10.1007/s10113-012-0299-0>, 2012.

590 Bianchi, T. S.: The role of terrestrially derived organic carbon in the coastal ocean: A changing paradigm and the  
591 priming effect, *Proceedings of the National Academy of Sciences*, 108, 19473–  
592 19481, <https://doi.org/10.1073/pnas.1017982108>, 2011.

- 593 Boetius, A., Ravenschlag, K., Schubert, C. J., Rickert, D., Widdel, F., Gieseke, A., Amann, R., Jørgensen, B. B.,  
594 Witte, U., and Pfannkuche, O.: A marine microbial consortium apparently mediating anaerobic oxidation of  
595 methane, *Nature*, 407, 623–626, <https://doi.org/10.1038/35036572>, 2000.
- 596 Comer-Warner, S. A., Ullah, S., Ampuero Reyes, W., Krause, S., and Chmura, G. L.: *Spartina alterniflora* has the  
597 highest methane emissions in a St. Lawrence estuary salt marsh, *Environmental Research: Ecology*, 1,  
598 011003, <https://doi.org/10.1088/2752-664X/ac706a>, 2022.
- 599 Conrad, R.: Importance of hydrogenotrophic, acetoclastic and methylotrophic methanogenesis for methane production  
600 in terrestrial, aquatic and other anoxic environments: A mini review, *Pedosphere*, 30, 25–  
601 39, [https://doi.org/10.1016/S1002-0160\(18\)60052-9](https://doi.org/10.1016/S1002-0160(18)60052-9), 2020.
- 602 Coolen, M. J. L. and Orsi, W. D.: The transcriptional response of microbial communities in thawing Alaskan  
603 permafrost soils, *Frontiers in Microbiology*, 6, 197, <https://doi.org/10.3389/fmicb.2015.00197>, 2015.
- 604 Costa, B.: Remote sensing analysis of recent coastal change and controlling factors in Tuktoyaktuk Peninsula  
605 (Beaufort Sea Coast, Canada), Master's dissertation, University of Lisbon, Repository of Lisbon University,  
606 2022.
- 607 Couture, N. J., Irrgang, A., Pollard, W., Lantuit, H., and Fritz, M.: Coastal erosion of permafrost soils along the Yukon  
608 Coastal Plain and fluxes of organic carbon to the Canadian Beaufort Sea, *Journal of Geophysical Research:*  
609 *Biogeosciences*, 123, 406–422, <https://doi.org/10.1002/2017JG004166>, 2018.
- 610 Cui, S., Liu, P., Guo, H., Nielsen, C. K., Pullens, J. W. M., Chen, Q., Pugliese, L., and Wu, S.: Wetland hydrological  
611 dynamics and methane emissions, *Communications Earth and Environment*, 5,  
612 1635, <https://doi.org/10.1038/s43247-024-01635-w>, 2024.
- 613 Bridgman, S. D., Cadillo-Quiroz, H., Keller, J. K., and Zhuang, Q.: Methane emissions from wetlands:  
614 biogeochemical, microbial, and modeling perspectives from local to global scales, *Global Change Biology*, 19,  
615 1325–1346, <https://doi.org/10.1111/gcb.12131>, 2012.
- 616 Dallimore, S. R., Wolfe, S. A., Matthews Jr., J. V., and Vincent, J.-S.: Mid-Wisconsinan eolian deposits of the  
617 Kittigazuit Formation, Tuktoyaktuk Coastlands, Northwest Territories, Canada, *Canadian Journal of Earth*  
618 *Sciences*, 34, 1421–1441, <https://doi.org/10.1139/e17-116>, 1997.
- 619 Elberling, B., Michelsen, A., Schädel, C., Schuur, E. A. G., Christiansen, H. H., Berg, L., Tamstorf, M. P., and  
620 Sigsgaard, C.: Long-term CO<sub>2</sub> production following permafrost thaw, *Nature Climate Change*, 3, 890–  
621 894, <https://doi.org/10.1038/nclimate1955>, 2013.
- 622 Froelich, P., Klinkhammer, G., Bender, M., Luedtke, N., Heath, G., Cullen, D., Dauphin, P., Hammond, D., Hartman,  
623 B., and Maynard, V.: Early oxidation of organic matter in pelagic sediments of the eastern equatorial Atlantic:  
624 suboxic diagenesis, *Geochimica et Cosmochimica Acta*, 43, 1075–1090, [https://doi.org/10.1016/0016-7037\(79\)90095-4](https://doi.org/10.1016/0016-7037(79)90095-4), 1979.
- 626 Fu, Q. A., Boutton, T. W., Ehleringer, J. R., and Flagler, R. B.: Environmental and developmental effects on carbon  
627 isotope discrimination by two species of *Phaseolus*, in: *Stable Isotopes and Plant Carbon-Water Relations*,  
628 Elsevier, 297–309, <https://doi.org/10.1016/B978-0-08-091801-3.50028-3>, 1993.
- 629 Galand, P. E., Yrjälä, K., and Conrad, R.: Stable carbon isotope fractionation during methanogenesis in three boreal  
630 peatland ecosystems, *Biogeosciences*, 7, 3893–3900, <https://doi.org/10.5194/bg-7-3893-2010>, 2010.

- 631 Guimond, J. A., Mohammed, A. A., Walvoord, M. A., Bense, V. F., and Kurylyk, B. L.: Saltwater intrusion intensifies  
632 coastal permafrost thaw, *Geophysical Research Letters*, 48,  
633 e2021GL094776, <https://doi.org/10.1029/2021GL094776>, 2021.
- 634 Heffernan, L., Cavaco, M. A., Bhatia, M. P., Estop-Aragonés, C., Knorr, K.-H., and Olefeldt, D.: High peatland  
635 methane emissions following permafrost thaw: enhanced acetoclastic methanogenesis during early  
636 successional stages, *Biogeosciences*, 19, 3051–3071, <https://doi.org/10.5194/bg-19-3051-2022>, 2022.  
637
- 638 Heslop, J. K., Walter Anthony, K. M., Sepulveda-Jauregui, A., Martinez-Cruz, K., Bondurant, A., Grosse, G., and  
639 Jones, M. C.: Thermokarst lake methanogenesis along a complete talik profile, *Biogeosciences*, 12,  
640 4317–4331, <https://doi.org/10.5194/bg-12-4317-2015>, 2015.  
641
- 642 Heslop, J. K., Walter Anthony, K. M., Winkel, M., Sepulveda-Jauregui, A., Martinez-Cruz, K., Bondurant, A., Grosse,  
643 G., and Liebner, S.: A synthesis of methane dynamics in thermokarst lake environments, *Earth-Science Reviews*,  
644 210, 103365, <https://doi.org/10.1016/j.earscirev.2020.103365>, 2020.
- 645 Heyer, J., Berger, U., Kuzin, I. L., and Yakovlev, O. N.: Methane emissions from different ecosystem structures of  
646 the subarctic tundra in Western Siberia during midsummer and during the thawing period, *Tellus B*, 54, 231–  
647 249, <https://doi.org/10.1034/j.1600-0889.2002.01280.x>, 2002.
- 648 Hill, P. R., Héquette, A., and Ruz, M.-H.: Holocene sea-level history of the Canadian Beaufort shelf, *Canadian Journal*  
649 *of Earth Sciences*, 30, 103–108, <https://doi.org/10.1139/e93-009>, 1993.
- 650 Hodgkins, S. B., Tfaily, M. M., McCalley, C. K., Logan, T. A., Crill, P. M., Saleska, S. R., Rich, V. I., and Chanton,  
651 J. P.: Changes in peat chemistry associated with permafrost thaw increase greenhouse gas production,  
652 *Proceedings of the National Academy of Sciences*, 111, 5819–5824, <https://doi.org/10.1073/pnas.1314641111>,  
653 2014.
- 654 Holm, S., Walz, J., Horn, F., Yang, S., Grigoriev, M. N., Wagner, D., Knoblauch, C., and Liebner, S.: Methanogenic  
655 response to long-term permafrost thaw is determined by paleoenvironment, *FEMS Microbiology Ecology*, 96,  
656 f1aa021, <https://doi.org/10.1093/femsec/f1aa021>, 2020.
- 657 Hornibrook, E. R. C., Longstaffe, F. J., and Fyfe, W. S.: Evolution of stable carbon isotope compositions for methane  
658 and carbon dioxide in freshwater wetlands and other anaerobic environments, *Geochimica et Cosmochimica*  
659 *Acta*, 64, 1013–1027, [https://doi.org/10.1016/S0016-7037\(99\)00321-X](https://doi.org/10.1016/S0016-7037(99)00321-X), 2000.
- 660 Hornibrook, E. R., Longstaffe, F. J., and Fyfe, W. S.: Spatial distribution of microbial methane production pathways  
661 in temperate zone wetland soils: stable carbon and hydrogen isotope evidence, *Geochimica et Cosmochimica*  
662 *Acta*, 61, 745–753, [https://doi.org/10.1016/S0016-7037\(96\)00368-7](https://doi.org/10.1016/S0016-7037(96)00368-7), 1997.
- 663 Hu, H., Chen, J., Zhou, F., Nie, M., Hou, D., Liu, H., Delgado-Baquerizo, M., Ni, H., Huang, W., Zhou, J., Song, X.,  
664 Cao, X., Sun, B., Zhang, J., Crowther, T. W., and Liang, Y.: Relative increases in CH<sub>4</sub> and CO<sub>2</sub> emissions from  
665 wetlands under global warming dependent on soil carbon substrates, *Nature Geoscience*, 17, 26–  
666 31, <https://doi.org/10.1038/s41561-023-01345-6>, 2024.
- 667 Hu, K., Issler, D., Chen, Z., and Brent, T.: Permafrost investigation by well logs, and seismic velocity and repeated  
668 shallow temperature surveys, Beaufort-Mackenzie Basin, Geological Survey of  
669 Canada, <https://doi.org/10.4095/293120>, 2013.

- 670 Hynes, S., Solomon, S. M., and Whalen, D.: GIS compilation of coastline variability spanning 60 years in the  
671 Mackenzie Delta and Tuktoyaktuk in the Beaufort Sea, Geological Survey of Canada Open File  
672 7685, <https://doi.org/10.4095/295579>, 2014.
- 673 Ionescu, D., Bizic-Ionescu, M., Khalili, A., Malekmohammadi, R., Morad, M. R., de Beer, D., and Grossart, H.-P.:  
674 A new tool for long-term studies of POM-bacteria interactions: overcoming the century-old Bottle Effect,  
675 Scientific Reports, 5, 14706, <https://doi.org/10.1038/srep14706>, 2015.
- 676 Irrgang, A. M., Bendixen, M., Farquharson, L. M., Baranskaya, A. V., Erikson, L. H., Gibbs, A. E., Ogorodov, S.  
677 A., Overduin, P. P., Lantuit, H., Grigoriev, M. N., and Jones, B. M.: Drivers, dynamics and impacts of  
678 changing Arctic coasts, Nature Reviews Earth and Environment, 3, 39–54, [https://doi.org/10.1038/s43017-  
679 021-00232-1](https://doi.org/10.1038/s43017-021-00232-1), 2022.
- 680 Jenrich, M., Wolter, J., Liebner, S., Knoblauch, C., Grosse, G., Giebel, F., Whalen, D., and Strauss, J.: Rising Arctic  
681 seas and thawing permafrost: uncovering the carbon cycle impact in a thermokarst lagoon system in the outer  
682 Mackenzie Delta, Canada, Biogeosciences, 22, 2069–2086, <https://doi.org/10.5194/bg-22-2069-2025>, 2025.
- 683 Jenrich, M., Angelopoulos, M., Liebner, S., Treat, C. C., Knoblauch, C., Yang, S., Grosse, G., Giebel, F., Jongejans,  
684 L. L., Grigoriev, M., and Strauss, J.: Greenhouse gas production and microbial response during the transition  
685 from terrestrial permafrost to a marine environment, Permafrost and Periglacial Processes, published online 4  
686 October 2024, <https://doi.org/10.1002/ppp.2251>, 2024.
- 687 Jones, E. L., Hodson, A. J., Thornton, S. F., Redeker, K. R., Rogers, J., Wynn, P. M., Dixon, T. J., Bottrell, S. H., and  
688 O'Neill, H. B.: Biogeochemical processes in the active layer and permafrost of a high Arctic fjord valley,  
689 Frontiers in Earth Science, 8, 342, <https://doi.org/10.3389/feart.2020.00342>, 2020.
- 690 Keuschnig, C., Larose, C., Rudner, M., Pesqueda, A., Doleac, S., Elberling, B., Björk, R. G., Klemmedtsson, L., and  
691 Björkman, M. P.: Reduced methane emissions in former permafrost soils driven by vegetation and microbial  
692 changes following drainage, Global Change Biology, 28, 3411–3425, <https://doi.org/10.1111/gcb.16137>, 2022.
- 693 Knittel, K. and Boetius, A.: Anaerobic oxidation of methane: progress with an unknown process, Annual Review of  
694 Microbiology, 63, 311–334, <https://doi.org/10.1146/annurev.micro.61.080706.093130>, 2009.
- 695 Knoblauch, C., Beer, C., Liebner, S., Grigoriev, M. N., and Pfeiffer, E.-M.: Methane production as key to the  
696 greenhouse gas budget of thawing permafrost, Nature Climate Change, 8, 309–  
697 312, <https://doi.org/10.1038/s41558-018-0095-z>, 2018.
- 698 Knoblauch, C., Beer, C., Sosnin, A., Wagner, D., and Pfeiffer, E.-M.: Predicting long-term carbon mineralization and  
699 trace gas production from thawing permafrost of Northeast Siberia, Global Change Biology, 19, 1160–  
700 1172, <https://doi.org/10.1111/gcb.12116>, 2013.
- 701 Kokelj, S. V., Lantz, T. C., Solomon, S., Pisarcic, M. F., Keith, D., Morse, P., Thienpont, J. R., Smol, J. P., and Esagok,  
702 D.: Using multiple sources of knowledge to investigate northern environmental change: regional ecological  
703 impacts of a storm surge in the Outer Mackenzie Delta, N.W.T., Arctic, 65,  
704 3, <https://doi.org/10.14430/arctic4214>, 2012.
- 705 Kramshøj, M., Albers, C. N., Holst, T., Holzinger, R., Elberling, B., and Rinnan, R.: Biogenic volatile release from  
706 permafrost thaw is determined by the soil microbial sink, Nature Communications, 9,  
707 3412, <https://doi.org/10.1038/s41467-018-05824-y>, 2018.

- 708 Kroeger, K. D., Crooks, S., Moseman-Valtierra, S., and Tang, J.: Restoring tides to reduce methane emissions in  
709 impounded wetlands: a new and potent blue carbon climate change intervention, *Scientific Reports*, 7,  
710 12138, <https://doi.org/10.1038/s41598-017-12138-4>, 2017.
- 711 La, W., Han, X., Liu, C.-Q., Ding, H., Liu, M., Sun, F., Li, S., and Lang, Y.: Sulfate concentrations affect sulfate  
712 reduction pathways and methane consumption in coastal wetlands, *Water Research*, 217,  
713 118441, <https://doi.org/10.1016/j.watres.2022.118441>, 2022.
- 714 Lacelle, D., Fontaine, M., Pellerin, A., Kokelj, S. V., and Clark, I. D.: Legacy of Holocene landscape changes on soil  
715 biogeochemistry: a perspective from paleo-active layers in northwestern Canada, *Journal of Geophysical  
716 Research: Biogeosciences*, 124, 2662–2679, <https://doi.org/10.1029/2018JG004916>, 2019.
- 717 Lantuit, H., Overduin, P. P., Couture, N., Wetterich, S., Aré, F., Atkinson, D., Brown, J., Cherkashov, G., Drozdov,  
718 D., Forbes, D. L., Graves-Gaylord, A., Grigoriev, M., Hubberten, H.-W., Jordan, J., Jorgenson, T., Ødegård, R.  
719 S., Ogorodov, S., Pollard, W. H., Rachold, V., and Vasiliev, A.: The Arctic coastal dynamics database: a new  
720 classification scheme and statistics on Arctic permafrost coastlines, *Estuaries and Coasts*, 35, 383–  
721 400, <https://doi.org/10.1007/s12237-010-9362-6>, 2012.
- 722 Lapham, L. L., Dallimore, S. R., Magen, C., Henderson, L. C., Powers, L. C., Gonsior, M., Clark, B., Côté, M., Fraser,  
723 P., and Orcutt, B. N.: Microbial greenhouse gas dynamics associated with warming coastal permafrost, western  
724 Canadian Arctic, *Frontiers in Earth Science*, 8, 582103, <https://doi.org/10.3389/feart.2020.582103>, 2020.
- 725 Li, Y., Wang, D., Chen, Z., Chen, J., Hu, H., and Wang, R.: Methane emissions during the tide cycle of a Yangtze  
726 Estuary salt marsh, *Atmosphere*, 12, 245, <https://doi.org/10.3390/atmos12020245>, 2021.
- 727 Liebner, S., Ganzert, L., Kiss, A., Yang, S., Wagner, D., and Svenning, M. M.: Shifts in methanogenic community  
728 composition and methane fluxes along the degradation of discontinuous permafrost, *Frontiers in Microbiology*,  
729 6, 356, <https://doi.org/10.3389/fmicb.2015.00356>, 2015.
- 730 Lim, M., Whalen, D., Martin, J., Mann, P. J., Hayes, S., Fraser, P., Berry, H. B., and Ouellette, D.: Massive ice control  
731 on permafrost coast erosion and sensitivity, *Geophysical Research Letters*, 47,  
732 e2020GL087917, <https://doi.org/10.1029/2020GL087917>, 2020.
- 733 Lipson, D. A., Zona, D., Raab, T. K., Bozzolo, F., Mauritz, M., and Oechel, W. C.: Water-table height and  
734 microtopography control biogeochemical cycling in an Arctic coastal tundra ecosystem, *Biogeosciences*, 9,  
735 577–591, <https://doi.org/10.5194/bg-9-577-2012>, 2012.
- 736 Lotem, N., Pellerin, A., Anthony, K. W., Gafni, A., Boyko, V., and Sivan, O.: Anaerobic oxidation of methane does  
737 not attenuate methane emissions from thermokarst lakes, *Limnology and Oceanography*, 68, 1316–  
738 1330, <https://doi.org/10.1002/lno.12349>, 2023.
- 739 Lovley, D. R. and Klug, M. J.: Sulfate reducers can outcompete methanogens at freshwater sulfate concentrations,  
740 *Applied and Environmental Microbiology*, 45, 187–192, <https://doi.org/10.1128/aem.45.1.187-192.1983>, 1983.
- 741 Mackay, J. R. and Dallimore, S. R.: Massive ice of the Tuktoyaktuk area, western Arctic coast, Canada, *Canadian  
742 Journal of Earth Sciences*, 29, 1235–1249, <https://doi.org/10.1139/e92-099>, 1992.
- 743 Maltby, J., Steinle, L., Löscher, C. R., Bange, H. W., Fischer, M. A., Schmidt, M., and Treude, T.: Microbial  
744 methanogenesis in the sulfate-reducing zone of sediments in the Eckernförde Bay, SW Baltic Sea,  
745 *Biogeosciences*, 15, 137–157, <https://doi.org/10.5194/bg-15-137-2018>, 2018.

- 746 Martens, C. S. and Berner, R. A.: Methane production in the interstitial waters of sulfate-depleted marine sediments,  
747 Science, 185, 1167–1169, <https://doi.org/10.1126/science.185.4157.1167>, 1974.
- 748 Martin, A. F., Lantz, T. C., and Humphreys, E. R.: Ice wedge degradation and CO<sub>2</sub> and CH<sub>4</sub> emissions in the  
749 Tuktoyaktuk Coastlands, Northwest Territories, Arctic Science, 4, 130–145, <https://doi.org/10.1139/as-2016-0011>, 2018.
- 751 Manson, G. K., Couture, N. J., and James, T. S.: CanCoast 2.0: data and indices to describe the sensitivity of Canada's  
752 marine coasts to changing climate, Geological Survey of Canada Open File  
753 8551, <https://doi.org/10.4095/314669>, 2019.
- 754 Murton, J. B.: Thermokarst-lake-basin sediments, Tuktoyaktuk Coastlands, western Arctic Canada, Sedimentology,  
755 43, 737–760, <https://doi.org/10.1111/j.1365-3091.1996.tb02023.x>, 1996.
- 756 Oh, Y., Zhuang, Q., Liu, L., Welp, L. R., Lau, M. C. Y., Onstott, T. C., Medvigy, D., Bruhwiler, L., Dlugokencky, E.  
757 J., Hugelius, G., D'Imperio, L., and Elberling, B.: Reduced net methane emissions due to microbial methane  
758 oxidation in a warmer Arctic, Nature Climate Change, 10, 317–321, [https://doi.org/10.1038/s41558-020-0734-](https://doi.org/10.1038/s41558-020-0734-z)  
759 z, 2020.
- 760 Oremland, R. S. and Polcin, S.: Methanogenesis and sulfate reduction: competitive and noncompetitive substrates in  
761 estuarine sediments, Applied and Environmental Microbiology, 44, 1270–  
762 1276, <https://doi.org/10.1128/aem.44.6.1270-1276.1982>, 1982.
- 763 Ozuolmez, D., Na, H., Lever, M. A., Kjeldsen, K. U., Jørgensen, B. B., and Plugge, C. M.: Methanogenic archaea and  
764 sulfate reducing bacteria co-cultured on acetate: teamwork or coexistence?, Frontiers in Microbiology, 6,  
765 492, <https://doi.org/10.3389/fmicb.2015.00492>, 2015.
- 766 Pellerin, A., Lotem, N., Walter Anthony, K., Eliani Russak, E., Hasson, N., Røy, H., Chanton, J. P., and Sivan, O.:  
767 Methane production controls in a young thermokarst lake formed by abrupt permafrost thaw, Global Change  
768 Biology, 28, 3206–3221, <https://doi.org/10.1111/gcb.16151>, 2022.
- 769 Penger, J., Conrad, R., and Blaser, M.: Stable carbon isotope fractionation by methylotrophic methanogenic archaea,  
770 Applied and Environmental Microbiology, 78, 7596–7602, <https://doi.org/10.1128/AEM.01773-12>, 2012.
- 771 Petersen, S. G. G., Kristensen, E., and Quintana, C. O.: Greenhouse gas emissions from agricultural land before and  
772 after permanent flooding with seawater or freshwater, Estuaries and Coasts, 46, 1459–  
773 1474, <https://doi.org/10.1007/s12237-023-01218-6>, 2023.
- 774 Poffenbarger, H. J., Needelman, B. A., and Megonigal, J. P.: Salinity influence on methane emissions from tidal  
775 marshes, Wetlands, 31, 831–842, <https://doi.org/10.1007/s13157-011-0197-0>, 2011.
- 776 Pönisch, D. L., Breznikar, A., Gutekunst, C. N., Jurasinski, G., Voss, M., and Rehder, G.: Nutrient release and flux  
777 dynamics of CO<sub>2</sub>, CH<sub>4</sub>, and N<sub>2</sub>O in a coastal peatland driven by actively induced rewetting with brackish water  
778 from the Baltic Sea, Biogeosciences, 20, 295–323, <https://doi.org/10.5194/bg-20-295-2023>, 2023.
- 779 Rampton, V. N.: Quaternary geology of the Tuktoyaktuk coastlands, Northwest Territories, Geological Survey of  
780 Canada, 1988.
- 781 Reebergh, W. S.: Oceanic methane biogeochemistry, Chemical Reviews, 107, 486–  
782 513, <https://doi.org/10.1021/cr050362v>, 2009.

- 783 Rosentreter, J. A., Maher, D. T., Erler, D. V., Murray, R. H., and Eyre, B. D.: Methane emissions partially offset blue  
784 carbon burial in mangroves, *Science Advances*, 4, eao4985, <https://doi.org/10.1126/sciadv.aao4985>, 2018.
- 785 Roy Chowdhury, T., Herndon, E. M., Phelps, T. J., Elias, D. A., Gu, B., Liang, L., Wullschleger, S. D., and Graham,  
786 D. E.: Stoichiometry and temperature sensitivity of methanogenesis and CO<sub>2</sub> production from saturated  
787 polygonal tundra in Barrow, Alaska, *Global Change Biology*, 21, 722–737, <https://doi.org/10.1111/gcb.12762>,  
788 2015.
- 789 Schuur, E. A. G., McGuire, A. D., Schädel, C., Grosse, G., Harden, J. W., Hayes, D. J., Hugelius, G., Koven, C. D.,  
790 Kuhry, P., Lawrence, D. M., Natali, S. M., Olefeldt, D., Romanovsky, V. E., Schaefer, K., Turetsky, M. R.,  
791 Treat, C. C., and Vonk, J. E.: Climate change and the permafrost carbon feedback, *Nature*, 520, 171–  
792 179, <https://doi.org/10.1038/nature14338>, 2015.
- 793 Segarra, K. E., Comerford, C., Slaughter, J., and Joye, S. B.: Impact of electron acceptor availability on the anaerobic  
794 oxidation of methane in coastal freshwater and brackish wetland sediments, *Geochimica et Cosmochimica Acta*,  
795 115, 15–30, <https://doi.org/10.1016/j.gca.2013.03.029>, 2013.
- 796 Sepulveda-Jauregui, A., Walter Anthony, K. M., Martinez-Cruz, K., Greene, S., and Thalasso, F.: Methane and carbon  
797 dioxide emissions from 40 lakes along a north–south latitudinal transect in Alaska, *Biogeosciences*, 12, 3197–  
798 3223, <https://doi.org/10.5194/bg-12-3197-2015>, 2015.
- 799 Sela-Adler, M., Ronen, Z., Herut, B., Antler, G., Vigderovich, H., Eckert, W., and Sivan, O.: Co-existence of  
800 methanogenesis and sulfate reduction with common substrates in sulfate-rich estuarine sediments, *Frontiers in*  
801 *Microbiology*, 8, 766, <https://doi.org/10.3389/fmicb.2017.00766>, 2017.
- 802 Sherr, E., Sherr, B., and Sigmon, C.: Activity of marine bacteria under incubated and in situ conditions, *Aquatic*  
803 *Microbial Ecology*, 20, 213–223, <https://doi.org/10.3354/ame020213>, 1999.
- 804 Skoog, D. A., West, D. M., Holler, F. J., and Crouch, S. R.: *Fundamentals of analytical chemistry*, 9th ed., Cengage  
805 Learning, Singapore, 2014.
- 806 Solomon, S. M., Whalen, D., Saper, R., and Mulvie, J.: Measuring the extent of storm surge flooding on the Mackenzie  
807 River Delta, Northwest Territories, Canada using synthetic aperture radar, in: *Proceedings of the 8th*  
808 *International Conference on Remote Sensing for Marine and Coastal Environments*, 2005.
- 809 Vardy, S. R., Warner, B. G., and Aravena, R.: Holocene climate effects on the development of a peatland on the  
810 Tuktoyaktuk Peninsula, Northwest Territories, *Quaternary Research*, 47, 90–  
811 104, <https://doi.org/10.1006/qres.1996.1869>, 1997.
- 812 Vaughn, L. J. S., Conrad, M. E., Bill, M., and Torn, M. S.: Isotopic insights into methane production, oxidation, and  
813 emissions in Arctic polygon tundra, *Global Change Biology*, 22, 3487–3502, <https://doi.org/10.1111/gcb.13281>,  
814 2016.
- 815 Steedman, A. E., Lantz, T. C., and Kokelj, S. V.: Spatio-temporal variation in high-centre polygons and ice-wedge  
816 melt ponds, Tuktoyaktuk Coastlands, Northwest Territories, *Permafrost and Periglacial Processes*, 28, 66–  
817 78, <https://doi.org/10.1002/ppp.1880>, 2017.
- 818 Tanski, G., Brüder, L., Wagner, D., Knoblauch, C., Lantuit, H., Beer, C., Sachs, T., Fritz, M., Tesi, T., Koch, B. P.,  
819 Haghypour, N., Eglinton, T. I., Strauss, J., and Vonk, J. E.: Permafrost carbon and CO<sub>2</sub> pathways differ at  
820 contrasting coastal erosion sites in the Canadian Arctic, *Frontiers in Earth Science*, 9,  
821 630493, <https://doi.org/10.3389/feart.2021.630493>, 2021.

- 822 Richter, T., Šantrůčková, H., Schädel, C., Schuur, E. A. G., Sloan, V. L., Turetsky, M. R., and Waldrop, M. P.: A pan-  
823 Arctic synthesis of CH<sub>4</sub> and CO<sub>2</sub> production from anoxic soil incubations, *Global Change Biology*, 21, 2787–  
824 2803, <https://doi.org/10.1111/gcb.12875>, 2015.
- 825 Treat, C. C., Wollheim, W. M., Varner, R. K., Grandy, A. S., Talbot, J., and Frolking, S.: Temperature and peat type  
826 control CO<sub>2</sub> and CH<sub>4</sub> production in Alaskan permafrost peats, *Global Change Biology*, 20, 2674–  
827 2686, <https://doi.org/10.1111/gcb.12572>, 2014.
- 828 Turetsky, M. R., Treat, C. C., Waldrop, M. P., Waddington, J. M., Harden, J. W., and McGuire, A. D.: Short-term  
829 response of methane fluxes and methanogen activity to water table and soil warming manipulations in an  
830 Alaskan peatland, *Journal of Geophysical Research: Biogeosciences*, 113,  
831 G03S05, <https://doi.org/10.1029/2007JG000496>, 2008.
- 832 Valdemarsen, T. B. and Kristensen, E.: Degradation of dissolved organic monomers and short-chain fatty acids in  
833 sandy marine sediment by fermentation and sulfate reduction, *Geochimica et Cosmochimica Acta*, 74, 1593–  
834 1605, <https://doi.org/10.1016/j.gca.2009.12.009>, 2010.
- 835 Whalen, D., Forbes, D. L., Kostylev, V., Lim, M., Fraser, P., Nedimović, M. R., and Stuckey, S.: Mechanisms,  
836 volumetric assessment, and prognosis for rapid coastal erosion of Tuktoyaktuk Island, an important natural  
837 barrier for the harbour and community, *Canadian Journal of Earth Sciences*, 59, 945–  
838 960, <https://doi.org/10.1139/cjes-2021-0101>, 2022.
- 839 Winfrey, M. R. and Ward, D. M.: Substrates for sulfate reduction and methane production in intertidal sediments,  
840 *Applied and Environmental Microbiology*, 45, 193–199, <https://doi.org/10.1128/aem.45.1.193-199.1983>, 1983.
- 841 Winkel, M., Sepulveda-Jauregui, A., Martinez-Cruz, K., Heslop, J. K., Rijkers, R., Horn, F., Liebner, S., and Walter  
842 Anthony, K. M.: First evidence for cold-adapted anaerobic oxidation of methane in deep sediments of  
843 thermokarst lakes, *Environmental Research Communications*, 1, 021002, <https://doi.org/10.1088/2515-7620/ab1042>, 2019.
- 845 Yang, S., Anthony, S. E., Jenrich, M., in 't Zandt, M. H., Strauss, J., Overduin, P. P., Grosse, G., Angelopoulos, M.,  
846 Biskaborn, B. K., Grigoriev, M. N., Wagner, D., Knoblauch, C., Jaeschke, A., Rethemeyer, J., and Liebner, S.:  
847 Microbial methane cycling in sediments of Arctic thermokarst lagoons, *Global Change Biology*, 29, 2714–  
848 2731, <https://doi.org/10.1111/gcb.16649>, 2023.
- 849 Ye, R., Keller, J. K., Jin, Q., Bohannon, B. J., and Bridgham, S. D.: Peatland types influence the inhibitory effects of  
850 a humic substance analog on methane production, *Geoderma*, 265, 131–  
851 140, <https://doi.org/10.1016/j.geoderma.2015.11.026>, 2016.
- 852 Yuan, J., Liu, D., Ji, Y., Xiang, J., Lin, Y., Wu, M., and Ding, W.: *Spartina alterniflora* invasion drastically increases  
853 methane production potential by shifting methanogenesis from hydrogenotrophic to methylotrophic pathway in  
854 a coastal marsh, *Journal of Ecology*, 107, 2436–2450, <https://doi.org/10.1111/1365-2745.13164>, 2019.
- 855 Zheng, J., RoyChowdhury, T., Yang, Z., Gu, B., Wullschleger, S. D., and Graham, D. E.: Impacts of temperature and  
856 soil characteristics on methane production and oxidation in Arctic tundra, *Biogeosciences*, 15, 6621–  
857 6635, <https://doi.org/10.5194/bg-15-6621-2018>, 2018.